A TIERED MICROCHIP SYSTEM FOR HIGH PURITY ISOLATION OF RARE CELLS FROM BLOOD

by

Onur Gur

A Dissertation

Submitted to the Faculty of Purdue University

In Partial Fulfillment of the Requirements for the degree of

Doctor of Philosophy

School of Electrical and Computer Engineering

West Lafayette, Indiana

December 2020

THE PURDUE UNIVERSITY GRADUATE SCHOOL
STATEMENT OF COMMITTEE APPROVAL

Dr. Cagri Savran, Co-Chair
School of Mechanical Engineering

Dr. Babak Ziaie, Co-Chair
School of Electrical and Computer Engineering

Dr. Saeed Mohammadi
School of Electrical and Computer Engineering

Dr. Thomas Talavage
School of Electrical and Computer Engineering

Approved by:
Dr. Dimitrios Peroulis

To all my teachers

ACKNOWLEDGMENTS

I would like to express my sincere thanks to my advisor Prof. Çağrı Savran for his continuous support and guidance over the years. He is a patient and kind advisor who is always there to listen and offer his help.

I would like to thank Prof. Babak Ziaie, Prof. Thomas Talavage, and Prof. Saeed Mohammadi for agreeing to be in my committee and providing invaluable feedback through my PhD.

I would like to thank all my lab mates at Savran Group over the years, Dr. Chun-Li Chang, Dr. Norman David Brault, Dr. Wanfeng Huang, Dr. Ben Chan, Rohil Jain, Yuan Zhong, and Maulee Sheth for always giving their honest feedback and providing suggestions to improve my research.

I would like to thank Dr. David Haas and Dr. Shelley Dowden from Indiana University OB-GYN department for their assistance with providing maternal blood samples.

I would also like to thank my parents Sibel and Can for always being there as I struggle through what life throws at me. I would also like to thank my in laws Toni and David for accepting me as part of their family and always making me feel welcome.

Finally, I would like to offer my dearest appreciation to my lovely wife Ariana who tirelessly supported me all throughout this journey.

TABLE OF CONTENTS

LIST OF TABLES

LIST OF FIGURES

ABSTRACT

Rare circulating cells are becoming a subject of interest due to their potential clinical applications to replace invasive procedures. Due their low presence in blood (as low as 1 in 1 ml of blood) various platforms are developed to capture and isolate them. Common limitations of current platforms include the inability to process large volumes of blood without an initial volume reduction step such as centrifugation, reliance on a single antibody for the capture, and the difficulty of releasing and retrieving the captured cells with high purity. A rare cell retrieval platform with high throughput operation and high purity retrieval is needed to capture these rare cells by processing large volumes of blood.

In this thesis study, we have developed a two-tiered microchip system to capture and retrieve rare cells from blood samples with high purity. The first module of the system is a high throughput microfluidic interface that is used to immunomagnetically isolate targeted rare cells from whole blood, and discard > 99.999% of the unwanted leukocytes. The second module is a microwell array that furthers the purification by magnetically guiding each cell into a separate well concurrently, and allows individual retrieval of each cell. Even though the system we have developed is applicable to many fields pertaining to rare cell capture, here we demonstrate the proof-of-concept using model cell lines that represent circulating fetal trophoblasts. We describe the design, operation as well as the experimental characterization of the system. Our characterization results show that the process can be completed within 145 minutes from the very beginning till the retrieval of a target cell, and can provide efficiencies and purities that are as high as 100%.

In order to demonstrate a real-world use case for our device, we present preliminary experiments done with blood samples from pregnant women. We show that we are able to retrieve candidate

fetal cells under 167 minutes. Future work will be focused on sequencing the candidate fetal cells retrieved from maternal samples to confirm their fetal origin as well as enhancing system performance in maximizing the number of cells captured.

1. INTRODUCTION

1.1 Motivation

Detection and molecular characterization of rare circulating cells in body fluids such as blood can have high significance for clinical applications due to their potential to replace invasive procedures [1–3]. One such type of cell, circulating tumor cells (CTCs) are used to develop liquid biopsy techniques to monitor tumor progression through enumeration of the cells in blood which is an alternative to invasive procedures such as surgical excisions or needle biopsies [2–4]. Additionally, genetic studies of the captured CTCs can reveal alterations in the genetic composition of the shed cells which can be different from the cells of the main tumor [4–6].

Similarly, the study of circulating fetal cells (CFCs) is viewed as alternative screening method in the field of prenatal diagnosis. The goal of prenatal diagnosis is to identify any genetic disorders in a fetus and guide the parents through various treatment options. The source of many genetic disorders, chromosomal abnormalities including aneuploidy, translocations, dislocations and deletions occur in 1 in every 150 live births [7]. More than 600 genetic disorders can be discovered by invasive procedures such as amniocentesis and chorionic villus sampling (CVS) [8].

Amniocentesis is performed at 15-16th week of pregnancy by insertion of a needle into amniotic sac and the obtaining of a sample of amniotic fluid (Figure 1.1a). This fluid contains cells of fetal origin which can be cultured and analyzed for genetic defects. Before the procedure, ultrasonic analysis is used to evaluate the position of the fetus to determine the optimal place and angle for the insertion of the needle. Common complications after an amniocentesis include miscarriages (~0.6-0.68%), amniotic fluid leakage, infection, and injury to the fetus by the puncture of the needle used for amniocentesis [8–13]. Further, should the expectant mother decide to terminate

the pregnancy after the 16th week, she necessarily has to go through a surgical procedure, whereas termination at earlier stages (e.g. 10th week) can be performed chemically by taking a pill.

CVS is performed by obtaining a sample of the chorionic villus which is part of the outer wall of the uterus called the placenta (Figure 1.1b). This region hosts trophoblasts which are of fetal origin. The sampling can be done transcervically or transabdominally and the procedure is performed around 10-12th week of pregnancy. Similar to amniocentesis, ultrasonic images are used to help with the positioning of the needle. While it has the advantage of being an earlier screening method than amniocentesis, it comes with a higher risk of miscarriage (~0.5-2%), limb defects and maternal bleeding [9–13].

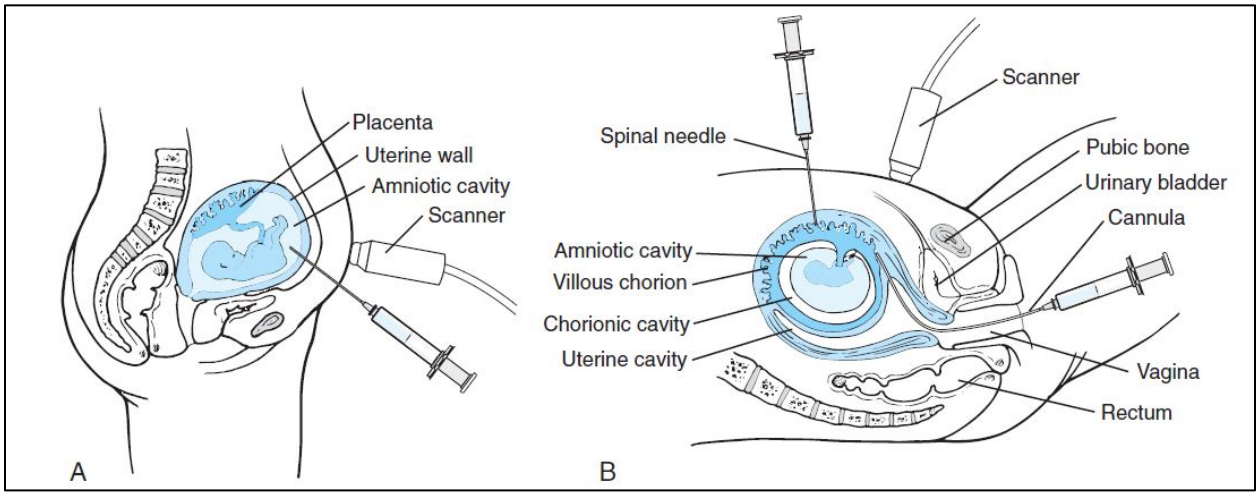

Figure 1.1. Schematics of a) Amniocentesis. b) Chorionic villus sampling [8]. The invasive nature of both procedures are conveyed with the inclusion of the needle and syringe on both schematics.

The difficulties associated with amniocentesis and CVS led to development of non-invasive methods. One non-invasive method is first and second trimester maternal serum screening combined with ultrasonic examinations [8,14]. First and second trimester screenings are done by obtaining maternal blood and taking ultrasonic images of the fetus. The quantity of certain proteins

(e.g. pregnancy-associated plasma protein A (PAPP-A), hormone human chorionic gonadotropin (hCG)) is correlated with the risk of trisomy 21 (down syndrome). The result of a combined first and second trimester screening can have a sensitivity of 95% and false positive rate of 5% for trisomy 21 [14]. While this method is effective in identifying trisomy 21, it falls short with other genetic conditions [8,14].

Another method involves retrieval of cell-free fetal DNA (cffDNA) from the plasma of the mother and analyzing it to detect genetic anomalies. Originated from trophoblasts, this DNA can account for approximately 10-20% of the cell free DNA found in the maternal plasma in the second trimester of gestation [14,15]. With this method, trisomies 13, 18, and 21 can be detected in more than 90% of the occurrences with false positive rates less than 0.25%, which makes this method more effective than the integrated screening test [14,16]. The shortcomings of this method is related to the fragmented nature of the fetal DNA, and the contamination from maternal DNA, which make it difficult to diagnose many other genetic disorders stemming from conditions such as mosaicism, small deletions, duplications or expansions [7,16–18]. For example, a condition called Fragile X, an expansion in the CGG repetitions in the X chromosome is nearly impossible to detect using cffDNA. This is because the size of a DNA strand in blood (~100-200 base pairs) will be too short to capture a 400-expansion of the CGG sequence (~1200 base pairs). Detecting Fragile X hence would require an intact genome.

An alternate non-invasive diagnostics method involves circulating fetal cells (CFCs). CFCs can be found as early as 6-8 weeks into pregnancy and can be retrieved from maternal blood without risking the fetus or the mother [19]. They are more effective in diagnosing chromosomal abnormalities in fetuses compared to cffDNA due to their intact fetal genome, and lack of

contamination from maternal DNA [20]. The major challenge regarding CFCs is that they are extremely rare (1-2 cells per milliliter of blood and in most cases even fewer), and they need to be obtained without contamination from white blood cells (WBCs) in order to be useful for downstream genetic analysis [21,22]. This has led to the development of several isolation methods for CFCs over the years.

The significant potential of genetically analyzing rare cell motivates us to develop a cell detection and retrieval system that can be used to target different types of cells and prepare them for genetic analysis in a robust manner. A previous version of our system was developed for only capture and quantification of rare cells [23,24], and not their retrieval. Here in this study, we focused on critical design modifications and additional modules that are required to further purify the captured cells by isolating them individually.

For this purpose, we developed a two a tiered microchip system for high purity isolation of rare cells from blood. This system adds additional functionalities to our previous work and due to its high-throughput operation and the resulting high purity target cells, we believe it has significant potential to contribute to clinical studies aiming to isolate and sequence rare cells from blood in a wide range of application from cancer to immunology. For the initial demonstration of the system's performance, we used prenatal diagnosis (a highly pressing problem in today's world) as a potential application and optimized our experiment conditions for the detection of CFCs.

1.2 Thesis Organization

Chapter 2 covers a literature review of the existing methods for detection of CFCs. Traditional methods used for categorizing cells are described, and their deficiencies when used for rare cell separation are noted. This is followed by more recent advancements in CFC capture that utilize

microfluidic methods. Devices from academia as well as commercial solutions from industry are included in this part. In addition to providing brief descriptions of these devices, their possible shortcomings are addressed as well.

In Chapter 3, we detail our own method of detecting and isolating rare cells, and explain how it overcomes the potential shortcomings of devices described in Chapter 2. We discuss our methods for dealing with the challenges of targeting rare cells and the need for their high purity retrieval. We detail how our system minimizes the sample preparation steps by processing a whole blood sample directly, without the need of any centrifugation, and is versatile enough to target a variety of antigens to achieve high recovery rate of cells.

Details related to fabrication, assembly, and characterization of the system are also given in Chapter 3. We detail the cleanroom fabrication workflow, the materials selected for building the microfluidic chambers, and the assembly procedure to form the final devices. We also describe our design choices and simulation results which were influenced by the forces within the system and the physical parameters such as the size of the cells, dimension and shape of the magnet, and the width of the fluidic chamber.

Experiments with cultured cells are covered in Chapter 4. Even though the system we have developed is applicable to many fields pertaining to rare cell capture, here we demonstrate the initial proof-of-concept using model cell lines that represent circulating fetal trophoblasts. Extravillous trophoblasts represent the genotype of the fetus (except in rare cases (1%) of confined placental mosaicism) and are expected to make an impact on the future of non-invasive prenatal diagnostics [25–28]. We detail our experimental methods and demonstrate that we are able to

isolate cells with high throughput and high purity, while being able to physically separate clusters of target cells from single target cells.

Chapter 5 details the experimental methods and results obtained from processing maternal blood. We discuss the minor modifications implemented to our detection protocol that is more suitable for detection of actual trophoblasts from the blood of expectant mothers. We were able to obtain fetal cell candidates from maternal samples with very high purity while keeping the total experiment time under 3 hours.

In Chapter 6, proposed future work is discussed. In order to demonstrate the proof of concept of performing genetic analysis on a single cell, we isolate a model cultured cell and show the copy number variation (CNV) results obtained from that cell. We demonstrate that target cells isolated with our system are not damaged and are indeed eligible for downstream genetic analysis. We also discuss potential improvements that may enhance the efficiency of the platform in maximizing the number of these extremely rare and precious cells.

2. LITERATURE REVIEW

2.1 Traditional Methods

Conventional methods for CFC enrichment include fluorescence activated cell sorting (FACS), magnetic activated cell sorting (MACS), and methods such as density gradient centrifugation and filtration that utilize the size difference between the targeted cells and the background cells (mostly WBCs) [25,29].

2.1.1 Fluorescence Activated Cell Sorting (FACS)

FACS method relies on specific biomarkers that target cells express to separate them from a sample fluid. Both the number of cells that have a certain biomarker and the quantitative distribution of the said biomarker from each cell can be retrieved after the analysis is complete. Fluorescent labeling is used to identify and quantify each biomarker.

In order for the cells to be analyzed sequentially, they are separated into droplets with hydrodynamic focusing. The droplets containing each cell are given a charge depending on their fluorescence levels and directed into separate containers after passing an electrical field (Figure 2.1a). This process may expose cells to high shear stresses which may affect their viability [29]. Additionally, the process of analyzing each cell individually makes this method very time consuming for samples with large number of cells [30,31]. The system is also made of costly equipment and requires trained personnel [25].

When used for fetal cell detection, samples analyzed with FACS method result in relatively low purity, i.e. a great number of unwanted cells which could necessitate additional enrichment steps.

For example, a study by Bianchi et al., where 20 ml of maternal blood was enriched for cells that express the transferrin receptor (TfR), yielded between 46,000 to 673,000 TfR^+ cells; of which an average of only 150 were determined to be the targeted cells by subsequent PCR and Southern blot analyses [32].

2.1.2 Magnetic Activated Cell Sorting

MACS is another method that rely on specific biomarkers that target cells express to separate them from a sample fluid. Unlike FACS where fluorescent labeling is utilized, MACS involves paramagnetic beads attached to cells which cause them to separate into different containers when passed through a magnetic field (Figure 2.1b).

Similar to FACS, samples analyzed with MACS result in relatively low purity: Experiments performed by Chen et al. where 20 target cells were spiked into 5 ml blood showed that negative enrichment by MACS result in recovery rates of around 35% with a total number of 27900 cells [15]. Hatt et al. used MACS by targeting the marker set CD105 and CD141 which resulted in 500,000 cells, only 0 to 18 of which were classified as candidate fetal cells after fluorescent labeling and manual scanning of the cells [25].

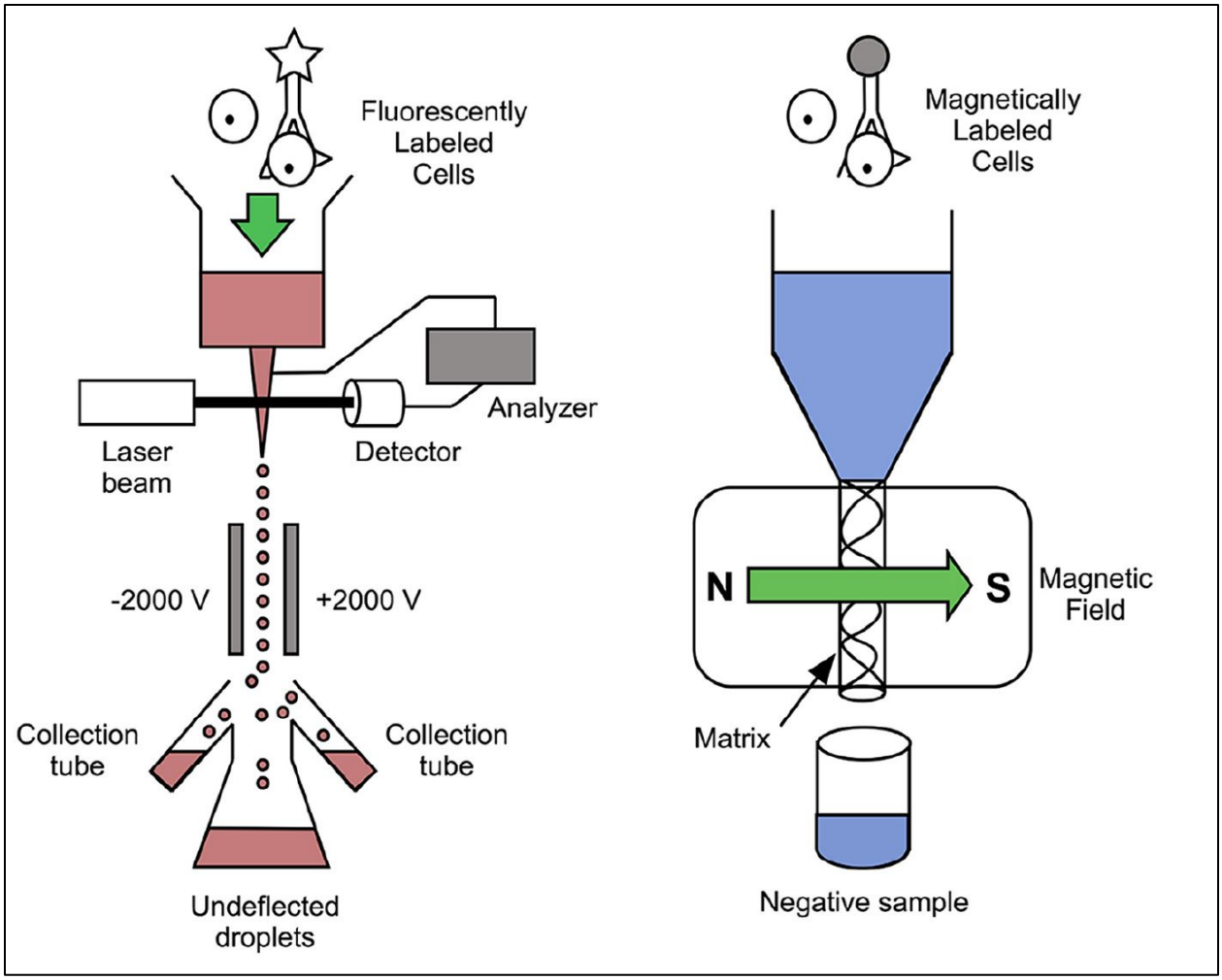

Figure 2.1. Schematic of a a) FACS, b) MACS systems [33].

2.1.3 Size-Based Separation Methods

One size-based method is centrifugation. A specific type of centrifugation called density gradient centrifugation aims to separate cells according to their density. With this method, Red Blood Cells (RBCs) can be separated from the solution. Due to the presence of WBCs in the resulting solution, an additional enrichment method is often needed. Common problems with density gradient centrifugation involve cell damage and cell loss of up to 40% due to migration to plasma layer [25,29,34,35].

Two studies by Calabrese et al. in 2011 and 2016 on fetuses with aneuploidy yielded a total of 50,000-100,000 cells of which only 4-9 were target cells per 25 ml blood, and 160,000-220,000 cells of which only 4-34 were target cells per 24 ml blood respectively [36,37].

Other size-based methods can involve filters and microfabricated channels that aim to separate target cells from the solution based on size alone. This method doesn't rely on specific biomarkers; however, it relies on the assumption that there are significant size and deformity differences between the targeted cells and other cells, which is not necessarily the case at all times.

Multiple groups used size-based detection to target CFCs. Vona et al. used polycarbonate filters with 8 μm to target CFCs and Mohamed et al. used successively narrowing channels to separate CFCs based on their size and deformation characteristics [38,39].

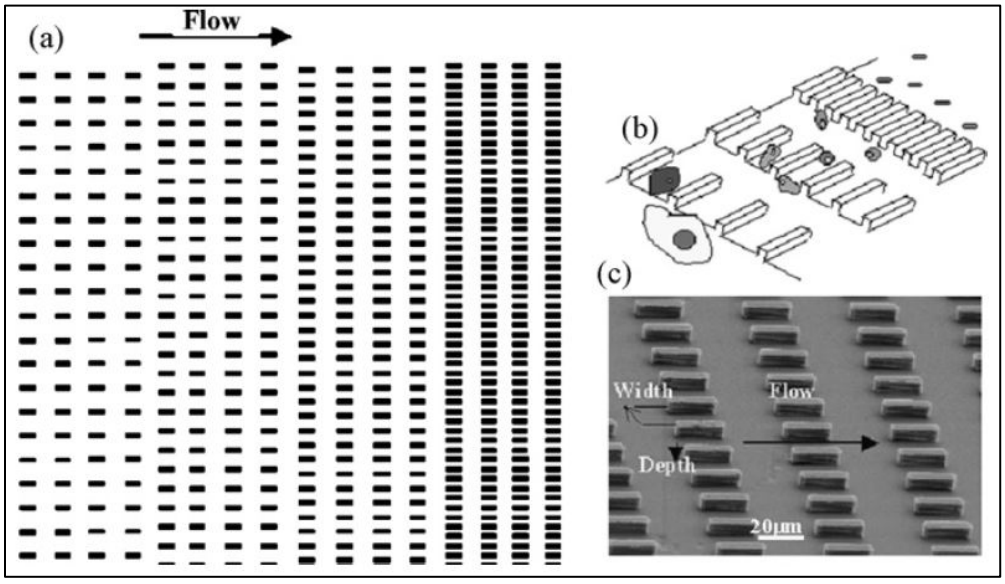

Figure 2.2. Schematic and SEM images of the narrowing channels developed by Mohamed et al. [40]

2.2 Microchip-Based Methods

Recently, various microfluidic devices were developed to further advance CFC isolation. Byeon et al. used a 2-step enrichment process to increase the purity of retrieved CFCs (Figure 2.3). A red blood cell hyperagregation step was used to facilitate the removal of white blood cells (WBCs) remaining in the supernatant ; followed by further purification by negative enrichment using a lateral magnetophoretic microseparator [41].

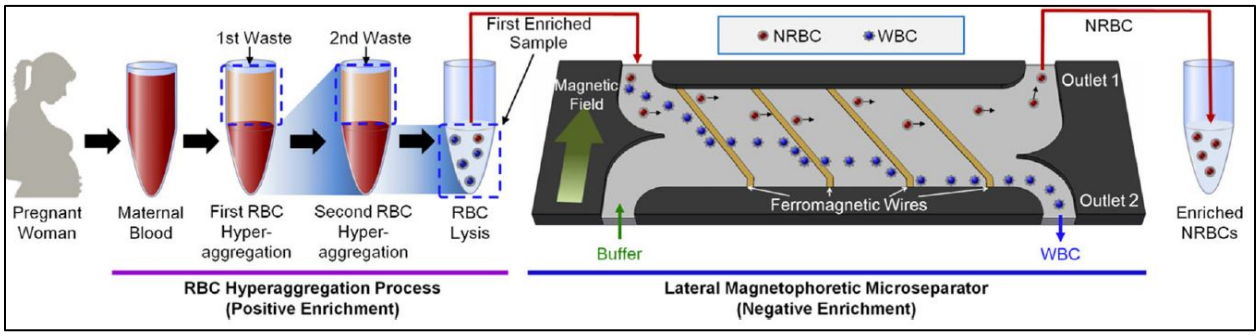

Figure 2.3. Schematic detailing the two separate enrichment steps of CFCs with the device developed by Byeon et al. [41]

Hou et al. developed the nano-Velcro microchips compatible with laser capture microdissection (LCM) technique to retrieve cells on a single cell resolution [26]. This chip is functionalized with anti-EPCAM antibodies which help capture the target cells. Due to the low flow rate needed to operate the chip (1 ml/hr) the sample is initially centrifuged with a density gradient solution. Beyond the slow flow rate, the system relies on affinity on a 2D surface which is sub-optimal (e.g. when compared to affinity in 3D). Besides, achieving tight control on functionalizing a 2D surface is extremely difficult, as is minimizing variability from one chip to another.

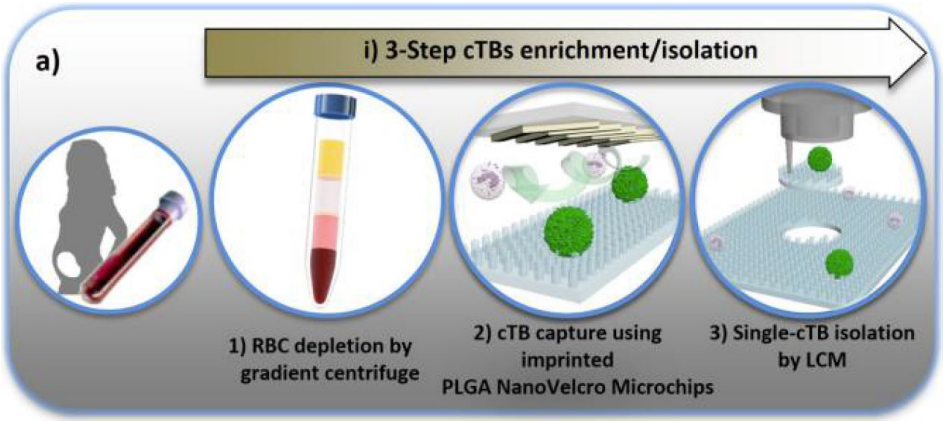

Figure 2.4. Schematic detailing the steps of CFC enrichment, capture, and isolation with the device developed by Hou et al. [26]

Winter et al. developed a device that utilizes inertial microfluidics to achieve high throughput separation of the CFCs (Figure 2.5). This method relies on the size differences between target cells and CFCs and therefore has the same disadvantages of the size-based methods discussed under traditional methods.

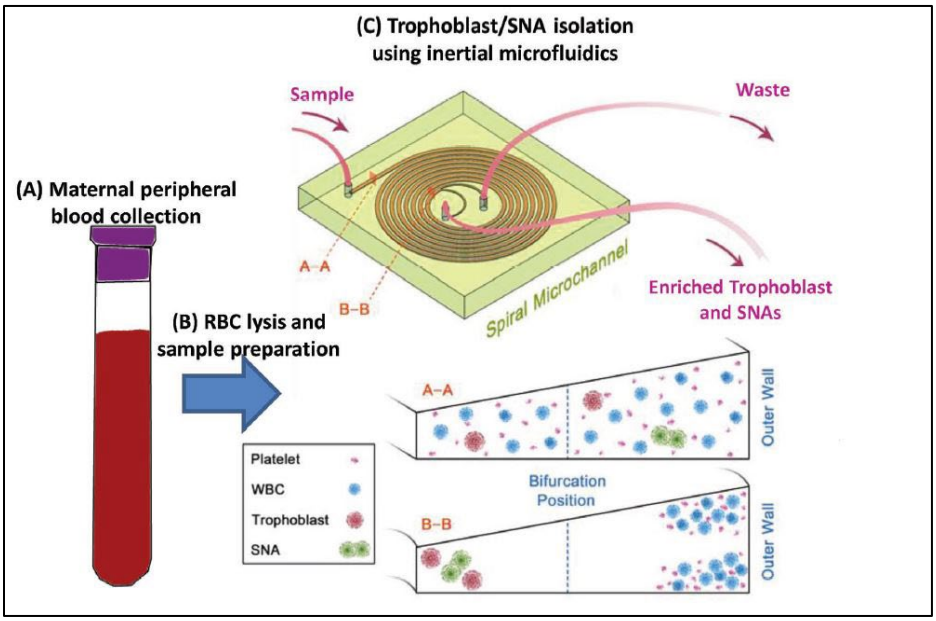

Figure 2.5. Schematic of the device from Winter et al. where the target cells are accumulated at the outside wall of the microchannel due to their size. [42]

Commercially, RareCyte developed a system which was demonstrated by Breman et al. where CFCs were isolated from blood, imaged automatically, and retrieved using a semi-automated picking routine [27,43,44]. While the automated parts of the workflow provides convenience, retrieval of the first target cell can take up to 15 hours [43].

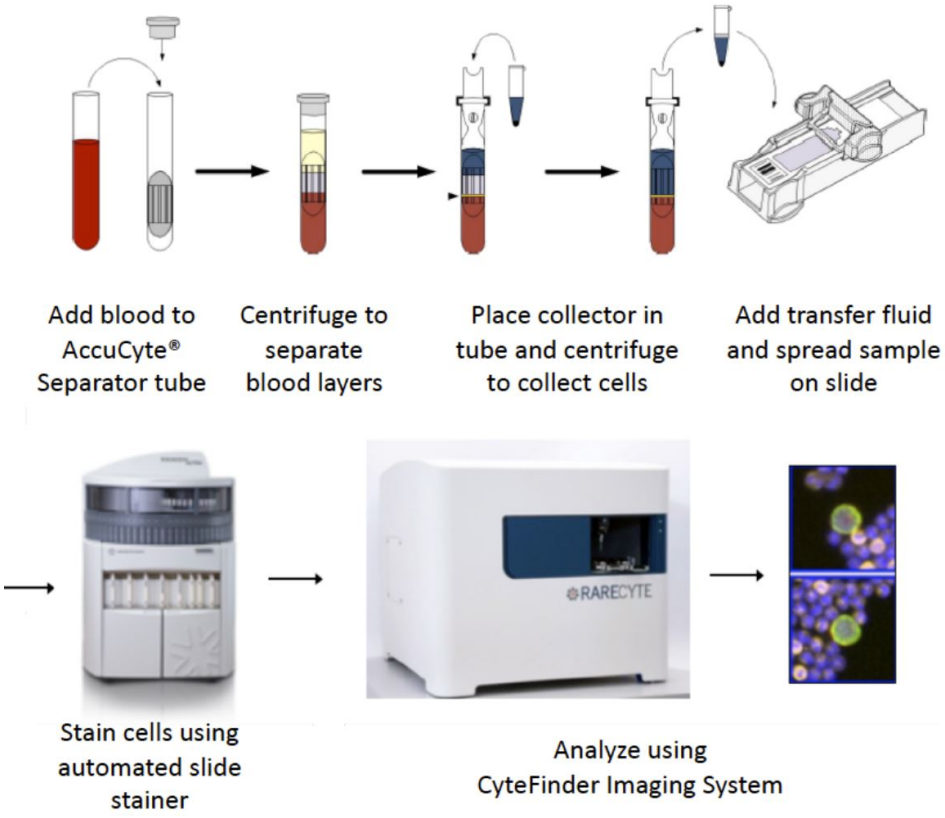

Figure 2.6. Workflow of the RareCyte cell capture system [44].

A common limitation of most microfluidic systems is that they generally cannot directly process a standard tube of blood sample (~8 ml) without an initial volume reduction step. This volume reduction is achieved either by centrifugation, which can lead to losses in cell viability, function, and number [25,29]; or red blood cell hyper aggregation, which can lead to losing precious target cells [41].

An additional common limitation in affinity-based cell capture methods is the use of a single antibody [26,45–47]. This hinders a platform's ability to capture cells that may not have a reduced expression of the targeted single antigen. Targeting a cocktail of antigens within the same device would mitigate this problem and circumvent the need to fabricate a different device for each antigen.

Upon successful initial isolation of target cells from a complex fluid, a critically important next step is to retrieve the cells individually for downstream analysis [41,45]. Most existing platforms release all captured cells from their surface in bulk into a single container. This hinders most types of analyses because the captured group of cells often contains non-targeted cells such as WBCs which reduces the overall purity by posing as background. Retrieving individual cells is therefore challenging since avoiding WBCs that surround a target cell often requires multiple attempts [27].

3. DESCRIPTION OF THE MICROCHIPS

3.1 Isolation System and Single Cell Retrieval Strategy

Our strategy involves two distinct microchip modules used in three steps. The first step is the isolation of the target cells from blood using a "porous chip" which we introduced previously [24]. Briefly, magnetic beads conjugated with antibodies are incubated with a blood sample to bind the surface antigens of the target cells. The mixture is then flowed through a fluidic chamber that contains a porous microchip that magnetically captures the target cells, clears out excess magnetic beads and washes away bulk of the unwanted white blood cells (WBCs) (Figure 3.1a).

The first step discards nearly 99.999875% of the WBCs. However, due to non-specific binding of the magnetic beads to WBCs, there are always some 100s of WBCs captured by the porous chip alongside the targeted rare cells. Any target cells retrieved at this stage would be mixed with WBCs, reducing the purity. An attempt to aspirate the targeted cells at this stage would also be problematic since all cells on the chip surface, including the unwanted WBCs, would be retrieved which would also reduce the overall purity.

Hence, in order to increase the purity further, the cells captured on the porous chip are transferred to a second module which accommodates a "well chip" which compartmentalizes all cells and allows their individual retrieval. The release of the cells from the porous chip is achieved by removing the magnet from underneath the porous chip, and initiating a buffer flow. Cells are next captured on the well chip surface once again by providing a magnetic field from below. Sweeping this magnetic field horizontally downstream directs the cells towards an array of microwells. Once a cell encounters a microwell, it falls into the microwell due to the downward magnetic force (Fig 1b).

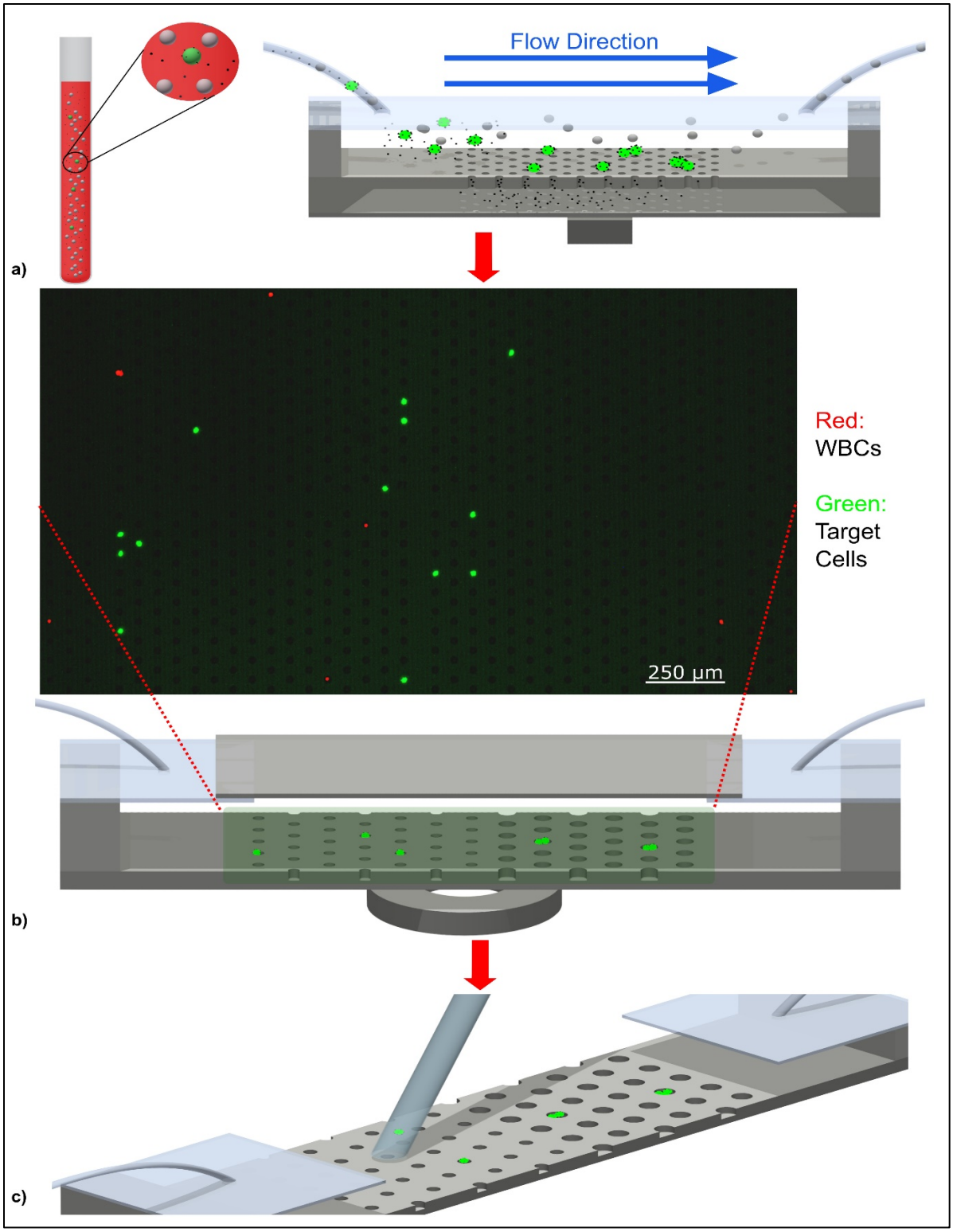

Figure 3.1. a) Isolation of target cells on porous chip. b) The target cells after they are transferred to well chip and separated in different wells. c) Retrieval of target cells using a micro pipette.

The diameter of microwells increase as cells move downstream. Hence, if a cell (or a group of cells) is too large to fit inside a microwell, it will eventually encounter and fall into a larger well downstream. This scheme not only enables a simple size-based classification of captured cells but also allows isolating each cell from all other cells, including those that were captured on the porous chip nonspecifically. Once each cell is captured in an individual well, the well chip is imaged via immunofluorescence to analyze and identify the location of the targeted cells (Figure 3.1b).

Finally, the top cover of the fluidic chamber that accommodates the well chip is opened up to retrieve each targeted cell with a micro pipette (Figure 3.1c).

3.2 Fabrication and Assembly of the Chips

3.2.1 Porous Chip

8 porous chips were fabricated on a 4 inch diameter, 500 μm thick <100> oriented double side polished Silicon wafer. The wafers were initially cleaned with a piranha solution containing sulfuric acid and hydrogen peroxide (H_2SO_4:H_2O_2 = 2:1) followed by a BOE (buffer oxide etch) wash to remove any oxide layer resulting from the piranha clean.

The micro apertures of the porous chip were defined by a photolithography step. AZ9260 (MicroChemicals GmbH) photoresist (PR) was used to spin coat the front side of the wafer starting at 500 rpm and ramping up to 3000 rpm for a total of 45 seconds. This process resulted ~8 μm thick photoresist to be used as a protective layer for the upcoming etching step. Following a soft bake on a hot plate at 90°C for 10 mins, the wafer was aligned and exposed by using the Karl Suss MA6.

The exposed PR was developed using AZ400K developer: DI water mixture (1:4 by volume) and the remaining PR was hard bake at 120°C.

The exposed silicon was etched with Deep Reactive Ion Etching (DRIE, STS ASE) for a 50 μm depth. The PR was then removed by placing the wafer overnight in a photoresist stripper (Baker, PRS-2000) at 90°C. Following another piranha and BOE clean, a layer of low stress silicon nitride (100 nm) was deposited on both sides of the wafer using low-pressure chemical vapor deposition (LPCVD). This nitride would act as a protective layer during the KOH etch of the back of the wafer.

The back opening was once again defined by a photolithography step. AZ9260 was spin-coated on both the front (to protect the already etched features from physical damage such as scratching against rough surfaces) and back sides of the wafer and the soft bake was performed in a PR baking oven at 90°C for 1 hour. The PR was back side alignment mode of Karl Suss MA6 optical aligner was utilized to define the features for wet etching. This was followed by developing the PR and hard baking at 120°C for 3 hours in the PR oven.

An SF6 plasma (Plasma Tech RIE 80) was used to dry etch the back of the wafer with the exposed nitride. Following that the remaining PR was removed and the wafer was cleaned with piranha and BOE.

To etch the defined back openings, a wet etch was performed on the wafer where it was placed in a 40% potassium hydroxide (KOH) solution at 80 °C. The etching rate was carefully monitored with frequents check of the depth of the back opening, and when the front side holes of the silicon became visible from the back side, the process was halted.

The remaining nitride layer was removed with a HF (diluted 1:10 with DI water) and the wafer was cleaned with piranha and BOE again to remove any contaminants from the etching process. The resulting wafer has 8 porous 40mm*20mm chips with a 2.76mm*8.58mm porous areas. The porous area defined by the DRIE was the surface where the target cells land and the excess beads are filtered through. The back etch done by the Plasma RIE defined the area under the porous surface that stored the excess beads during a detection experiment. The entire fabrication process is shown in Figure 3.2a-f and the SEM images of the micro-apertures on a fabricated chip are shown in Figure 3.2g-h [48].

The porous chip is housed in a fluidic chamber that is comprised of multiple components shown in Figure 3.2i [49]. The fluidic chamber was defined by a 1 mm thick PDMS with a 3.8 mm by 30 mm groove. The top was covered by a 1 mm thick glass which houses the inlet and outlet tubes. The openings for the tubes were drilled with a diamond tip and the tubes were attached with epoxy and super glue. The transparency of the glass also enabled the observation of cells on the porous surface without opening the chamber.

The bottom of the porous chip was sealed by a 0.1mm thick PDMS and a transparency sheet (3M PP2500, 0.1 mm thick). This was necessary to collect any magnetic beads and other impurities that fall through the apertures of the porous chip.

Finally, the entire structure was sandwiched between a top and bottom 3mm thick acrylic sheet (Grainger, 1UNZ5) to ensure the sealing of the entire chamber. The covers were cut to house machine screw and nuts which were fastened to create a hermetic seal. The bottom acrylic has a middle opening that houses the magnet, and the top acrylic has an opening to enable observation

of the porous chip surface. Acrylic was chosen because of its compatibility with laser cutters and its ability to withstand stresses caused by the machine screw and nut pairs.

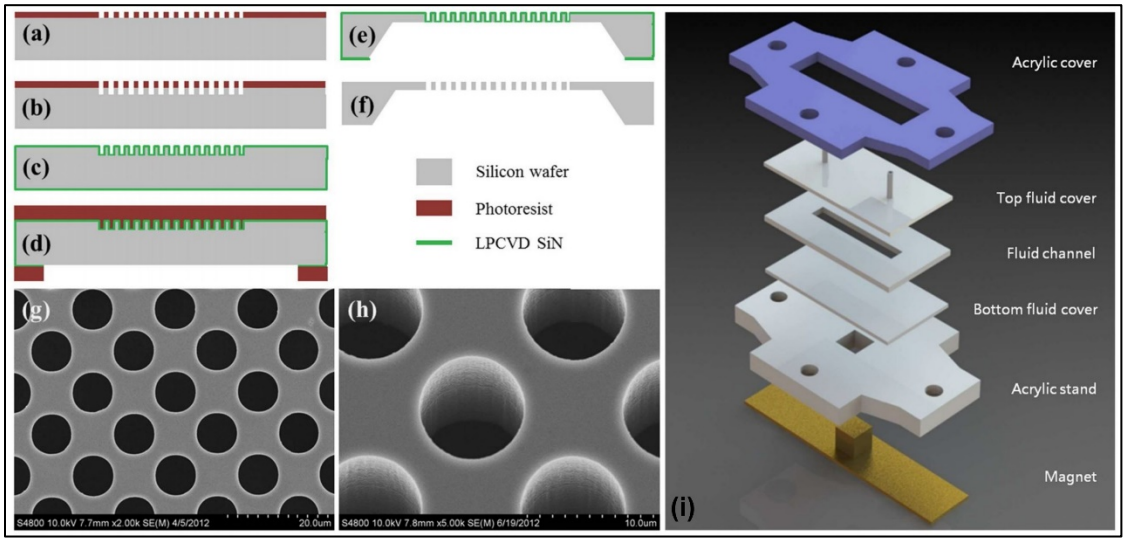

Figure 3.2. a-f) The fabrication process of the porous chips [48]. g-h) The resulting SEM image of the macroapertures on the front side of the porous chip [48]. i) Components of the porous chamber in an exploded view [49].

3.2.2 Well Chip

For the well chip, following the piranha and BOE clean, a 500 µm thick <100> oriented single side polished Si wafer was coated with AZ 9260 positive photoresist at 3000 rpm to define the areas with wells. After a 10 min soft bake at 90°C, the wafer was aligned and exposed by the Karl Suss MA6. The PR was developed by a AZ400K developer: DI water mixture (1:4 by volume). A 30 min hard bake at 120°C was used to turn the remaining PR to a protective layer for the etching step.

To etch the wells, Deep Reactive Ion Etching was used to obtain the 20 µm deep wells. The ability to do an anisotropic etch at a consistent etching rate made DRIE as ideal instrument for this step as a constant depth (20 µm) was required throughout the entire Si wafer. The remaining photoresist

was removed by keeping the wafer in a photoresist stripper (Baker, PRS-2000) overnight at 90°C. Finally, the wafer was once again cleaned with piranha to remove any PR residue and dipped in BOE to remove any oxide layer. This process resulted in 4 well chips in a wafer, each with the dimensions of 51mm*26mm. The inner area that contained the micro wells measured 20mm*7mm. The SEM images of a progressively magnified array of wells is presented in Figure 3.3e. Individual well chips were collected by cutting the wafer with a dicing saw (Disco DAD-2H/6).

The wells are separated into individual islands (0.6mm*0.9mm) that are fully visible under 10x magnification. The formation of the wells is staggered along the direction of fluidic flow which increases the likelihood of a cell encountering a well. Each island is labeled with a letter and each well can be identified by its row, column and label. For example, the island shown in Figure 3.3e is labeled 'E2' and a well on the top left can identified as the well at '1st row, 1st column of E2'. This helps users keep track of the location of fluorescently labeled target cells even after a possible photobleaching experienced by the said cells. Once the locations of target cells are recorded during a fluorescent analysis, users can switch to bright filed for easier operation of the micropipette to return and pick the cells.

For the well chip, a 1mm thick PDMS with a grove of 10mm by 46 mm was used to define the fluidic chamber. On top of this, a 0.5 mm thick PETG (Polyethylene Terephthlate Glycol-Modified) Sheet (Small Parts, VIS-060335-G-01) with a grove of 10mm by 30mm was placed as a top cover. Unlike glass which was the material of choice for the top cover of the porous chamber, PETG was preferred for the well chamber due to the need to cut an opening on it which could be achieved by a laser cutter. This opening would enable the micro pipette to be dipped on to the surface of the well chip. This PETG layer also houses the inlet and outlet tubes. The holes for those tubes were

similarly defined by a laser cutter and the tubes themselves were attached with super glues and epoxy.

The groove on the PETG was sealed by a 2mm PDMS, which can be peeled off to access the chamber. PDMS has multiple advantages as the material of choice for a top sealant. The flexibility of PDMS makes it easier to peel it off slowly when accessing the fluidic chamber. The hydrophobic nature of PDMS prevents pulling the fluid inside the fluidic chamber as it's moved away from the top of the chamber, leading to minimum disturbance of the content inside the well chip while it is being opened. Finally, PDMS is transparent which means the cells on top of the wells can be observed without removing the top cover of the well chamber if that is desired.

This structure was sandwiched between a 2-piece 3 mm thick top acrylic and a 4.4 mm thick bottom acrylic (Grainger, 1UNZ5 and 1UNZ6). These pieces had openings to fit machine screws and nuts to provide a hermetic seal. The top acrylic had an outer piece that sealed the fluidic chamber while the inner part was made removable to access the cells for retrieval. The middle part specifically sealed the middle opening of the PETG cover and the PDMS above it. Because the middle cover had its own set of screws and nuts, in the event of opening chamber, the seal between the PDMS spacer and the well chip would still hold due to the pressure from the outer piece. This would prevent any fluid leakage out of the chamber when the contents of the well chip were observed with an open middle top.

The bottom acrylic cover has an opening that fits the magnet. This opening is bigger than the magnet and covers the entire well area so that a magnet can be swept underneath the well chip to magnetically move cells along the entirety of the well area. The exploded view of all the components that make up the well chamber can be seen in Figure 3.3f.

The patterning done on the acrylic sheet, PDMS, PETG and transparent sheet for porous and well chambers were all done with a Universal Laser Systems Professional Series Laser Cutter.

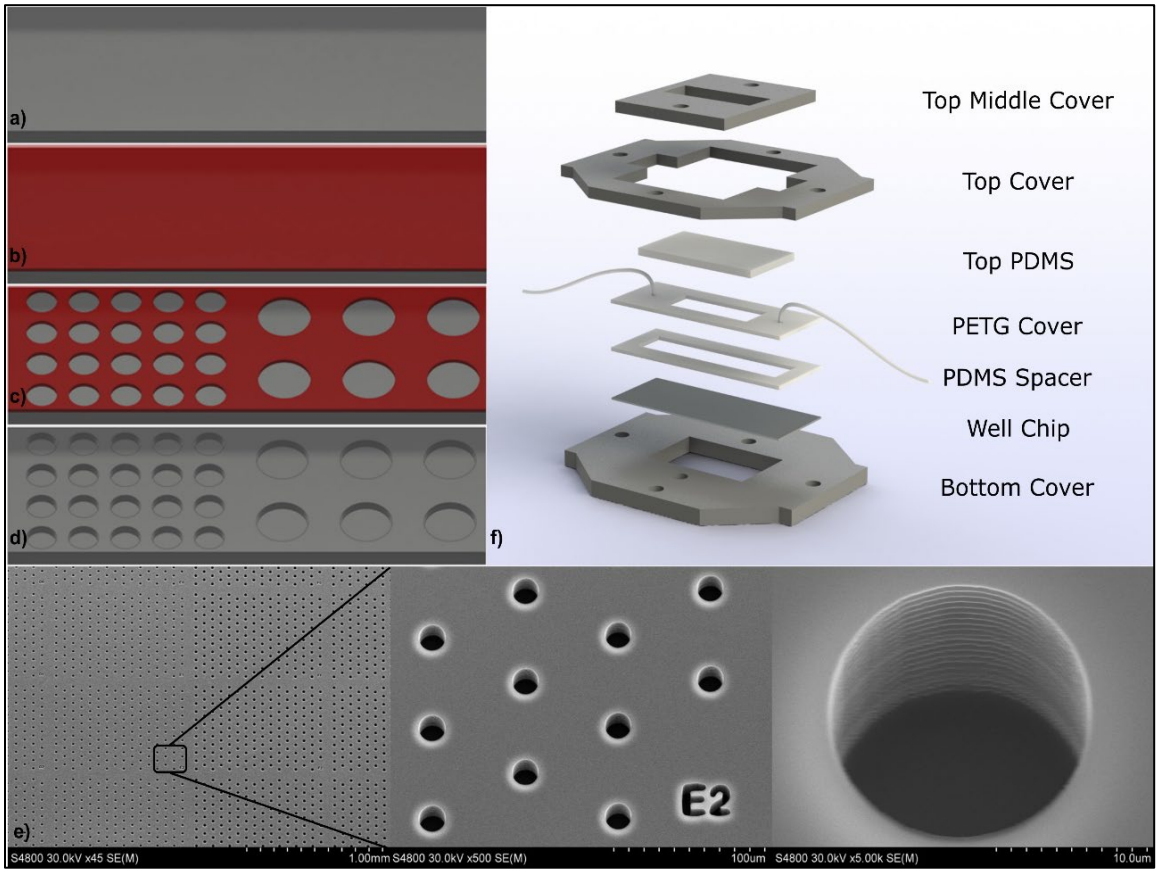

Figure 3.3 a-d) The fabrication process of the well chips. e) SEM images of the wells. f) Components of the well chamber in an exploded view.

3.3 Well Chip System Design and Modeling

An important feature of the well chip operation is its robustness and overall simplicity. All cells and cell clusters are distributed into their respective wells simultaneously, and separated by size using only a horizontally moving magnetic field. This is achieved manually by the user moving the magnet by hand (Figure 3.4a-b). This leads to a quick and robust process that does not require monitoring cell motion under a microscope. We describe below various parameters that influenced its design and performance.

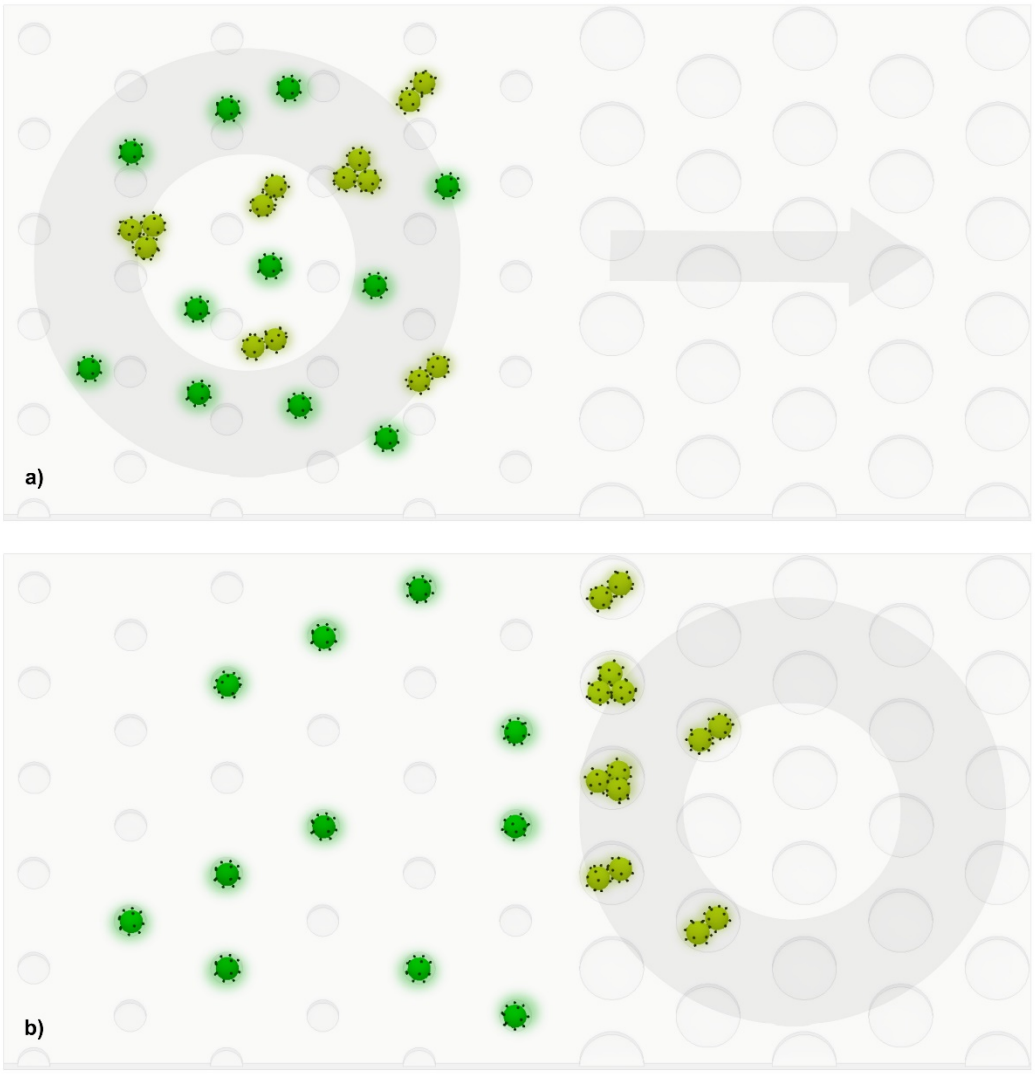

Figure 3.4 a) Before magnet sweep: The magnet is upstream (to the left) and the cells are distributed randomly. b) After magnet sweep: Magnet has moved downstream (to right) and cells and clusters are distributed into individual wells.

3.3.1 Well Size

In order to determine the size of the wells, the diameters of 40 cultured JEG3 were recorded by microscopic observation. The diameters of JEG3s ranged from 11.3 μm to 18.3 μm (Figure 3.5a). WBC diameters ranged from 9-20 μm depending on their type and red blood cell (RBC) diameters range from 6-8 μm [50,51]. The well sizes were accordingly chosen to be 15, 20, 30, and 60 μm.

The 15 μm and 20 μm wells were designed to hold single cells while 30 μm and 60 μm wells were added to hold cells in clusters (both target cells and WBCs). RBC diameter was not considered in well diameter decisions due to the availability of RBC lysing solutions that can effectively remove majority of RBCs. Additionally, lack of nucleus and DNA material in RBCs indicate that they wouldn't act as a contaminant in the event of a DNA analysis of any target cell picked together with RBCs.

The depth of the wells was chosen as 20 μm. It was observed that for wells less than 20 μm deep, some cells were able to roll out of the well due to the drag force by the fluid flow in the chamber, causing loss of target cells. On the other hand, wells deeper than 20 μm led to the stacking of target cells in a single well. This is undesirable because the fluorescent signal from the top cell would often mask the signal from the bottom cell, leading to an inaccurate sum of target cells.

3.3.2 Well to Well Distance

The distance between neighboring wells, D_{ww} was determined based on the diameter of the micro pipette tip that was used (Figure 3.5b) with the primary design goal being that the tip cross-section should only coincide with a single well while minimizing the distance between wells. A densely packed grid of wells is essential to isolating the target cells and impurities into physically separate containers. It is equally important to be able to retrieve contents of only a single well during the retrieval process with the micropipette. Assuming a conservative scenario where the pipette tip fully covers a well while being tangent to a neighboring well (Figure 3.5b), and D_w (diameter of the well) to be less than D_p (the diameter of the pipette tip), we determined the minimum well-to-well distance to be equal to the diameter of the pipette tip which for our setup was 50 μm.

An additional 10 µm was added to account for uncertainties and 60 µm was chosen as the final value of D_{ww}.

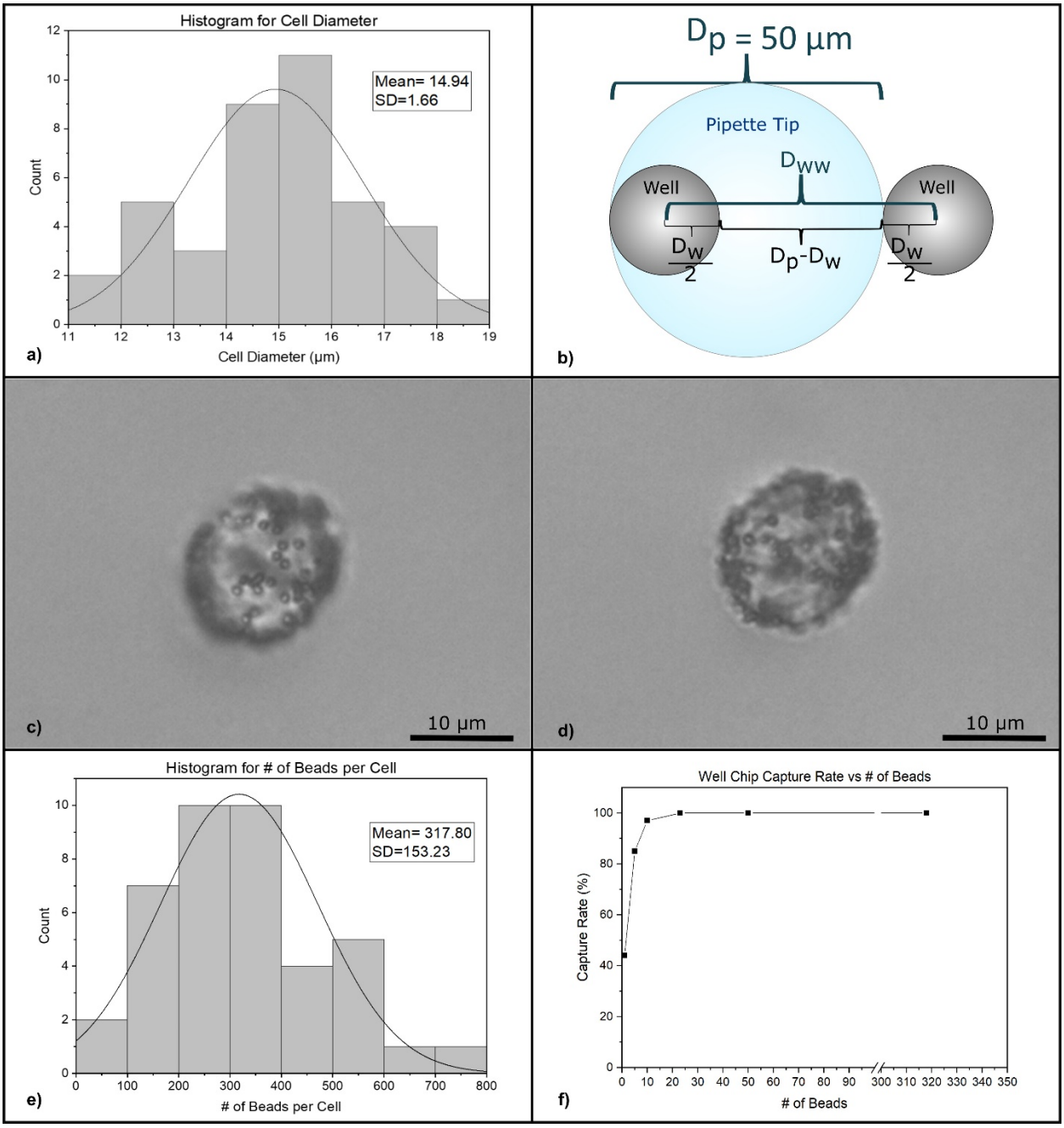

Figure 3.5. a) The distribution of the cell diameters. b) The distance between wells in relation to pipette tip. c-d) Bright field image of a JEG3 cell with beads under 2 different focus. e) Detection rate on well chip vs the number of beads on a cell. f) The distribution of # of beads per cell.

3.3.3 Magnet Type

Commercially available N52 neodymium magnets were used for their ease of use in a biosafety cabinet. Unlike an electromagnet, neodymium magnets don't require power source and wiring which makes and experiment setup simpler and safer. Their availability in different geometries and sizes made it easier to locate a magnet that was compatible with our existing microfluidic chamber designs.

In order to systematically determine the most appropriate type of magnet for distributing cells into individual wells, a few different commercial magnets were investigated via a numerical simulation. The particle tracing module of COMSOL was used to calculate the cell-to-cell separation of 100 target cells introduced into a channel with a width of 10 mm, and thickness of 1.5 mm, under a fluidic flow rate of 2 ml/min. The goal of the simulation was to identify a magnet which was strong enough to pull all the target cells on the surface of the well chip while keeping them as separated from each other as possible. The separation of the target cells on the surface increase their chances of falling into separate wells.

To track the movement of cells, the forces that primarily influence them were identified and calculated. These forces are magnetic force ($\overrightarrow{F_m}$), fluidic drag force ($\overrightarrow{F_d}$), gravity ($\overrightarrow{F_g}$), and buoyancy forces ($\overrightarrow{F_b}$) and are related with the following equation:

$$m\frac{d\vec{v}}{dt} = \overrightarrow{F_m} + \overrightarrow{F_d} + \overrightarrow{F_g} + \overrightarrow{F_b}$$

Where m and *v* are the mass and velocity of the cell- magnetic bead complex.

The force on magnetic beads (Thermo Fisher Scientific, MA1-10361) was expressed using the following equation which is derived from the magnetic force acting on a point-like magnetic dipole [52]:

$$\overrightarrow{F_m} = N\frac{V_p\chi}{2\mu_0}\nabla(\vec{B}\cdot\vec{B})$$

Here *N* is the number of beads on a cell. In order to input the correct number of beads on a cell, cells conjugated with beads were observed under bright field microscopy. Due to their large diameter (1 μm) most individual beads were visible and accounted for by switching through different focus points (Figure 3.5c-d). After analyzing 40 cells, it was determined that the cells had an average of 318 beads per cell (Figure 3.5e) which is well above the 23 beads per cell needed to ensure 100% capture rate on well chip (Figure 3.5e, determined by COMSOL).

B is the magnetic flux density [T]. It's calculated by using the "Magnetic fields, no currents" module of COMSOL. The parameters needed to calculate the magnetic flux density are the material related residual induction Br_{max} and relative permittivity μ_r of neodymium which are 1.48 T (for N52 grade) and 1.05 respectively. The resulting magnetic flux density for the cross section of a ring magnet is given in Figure 3.6a.

V_p is the volume of the bead (4.19 μm^3), χ is the relative susceptibility (0.35) [53,54], and μ_0 is the vacuum permeability ($1.257\cdot10^{-6}$ H/m).

The z component of the resulting force is shown in Figure 3.6b. The negative value indicated that the cell-bead complex is being pulled on the surface of the well chip. It is maximized around the edges of the magnet and reduces to zero within millimeters away from the magnet.

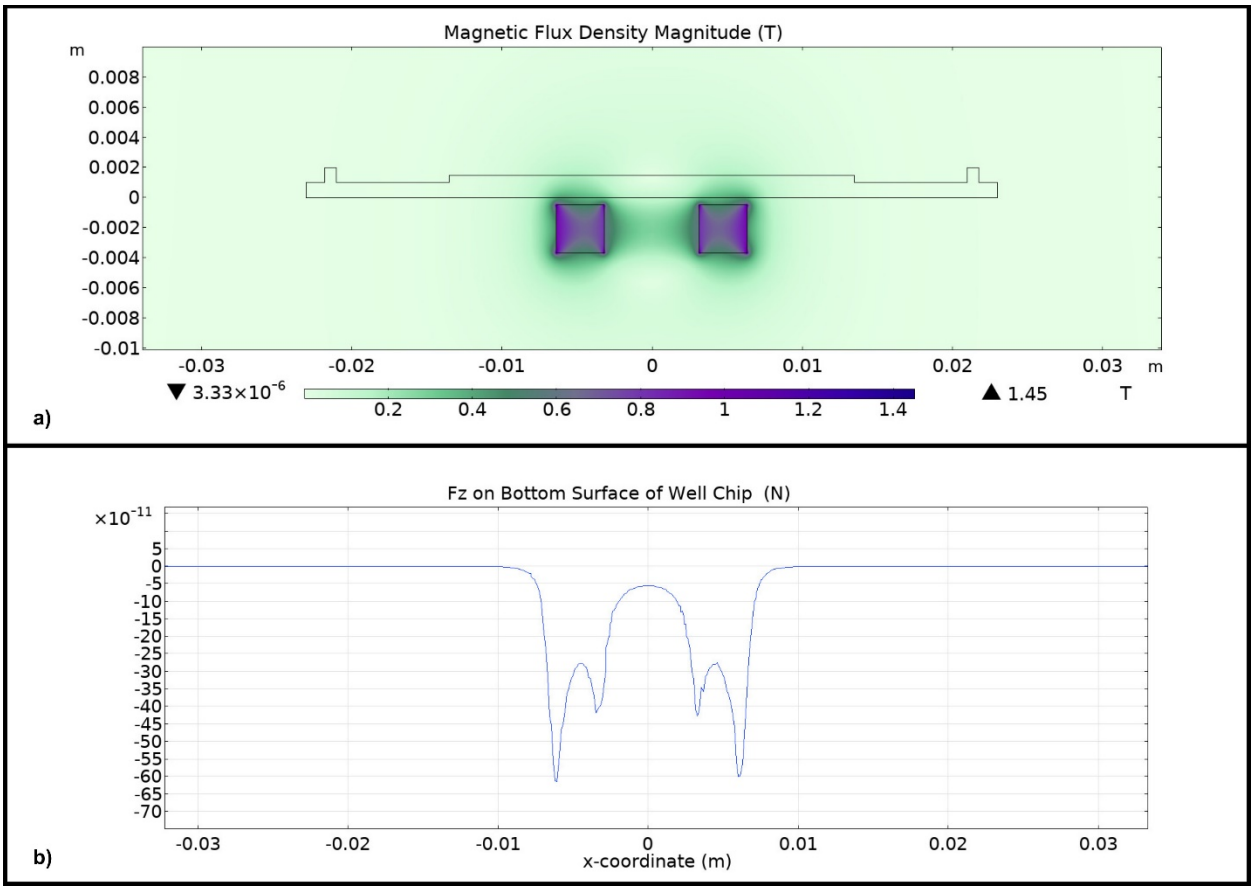

Figure 3.6. a) Magnetic flux density of a ring magnet. b) Magnetic force of the same magnet in the z direction.

The drag force on a cell was expressed by the following Stokes' drag equation [55]:

$$\overrightarrow{F_d} = 6\pi\mu R\upsilon$$

where μ is the dynamic viscosity ($1.05 \cdot 10^{-3}$ Pa·s for PBS), R is the radius of the cell, (7.5 μm), and υ is the flow velocity relative to the cell (calculated in COMSOL).

In order to calculate υ, information about the flow profile in the fluid chamber is needed. Reynolds number, a dimensionless quantity, is used to determine the flow pattern and has the following equation:

$$Re = \frac{\rho u L}{\mu}$$

Where ρ is the density of the fluid [1010 kg/m^3 for PBS], u is the velocity of the fluid [m/s], L is the characteristic length [m] ($\frac{2*w*l}{w+l}$ for a rectangular cross section with width w and length l), and μ is the dynamic viscosity of the fluid [Pa*s].

For a rectangular cross section of 1.5 mm * 1 mm and a flow rate of 2ml/min, the Reynolds Number becomes 12.8 which puts it strictly in the laminar flow region. Therefore, the laminar flow module of COMSOL was used to calculate the flow velocity inside the fluidic chamber (Figure 3.7a-b).

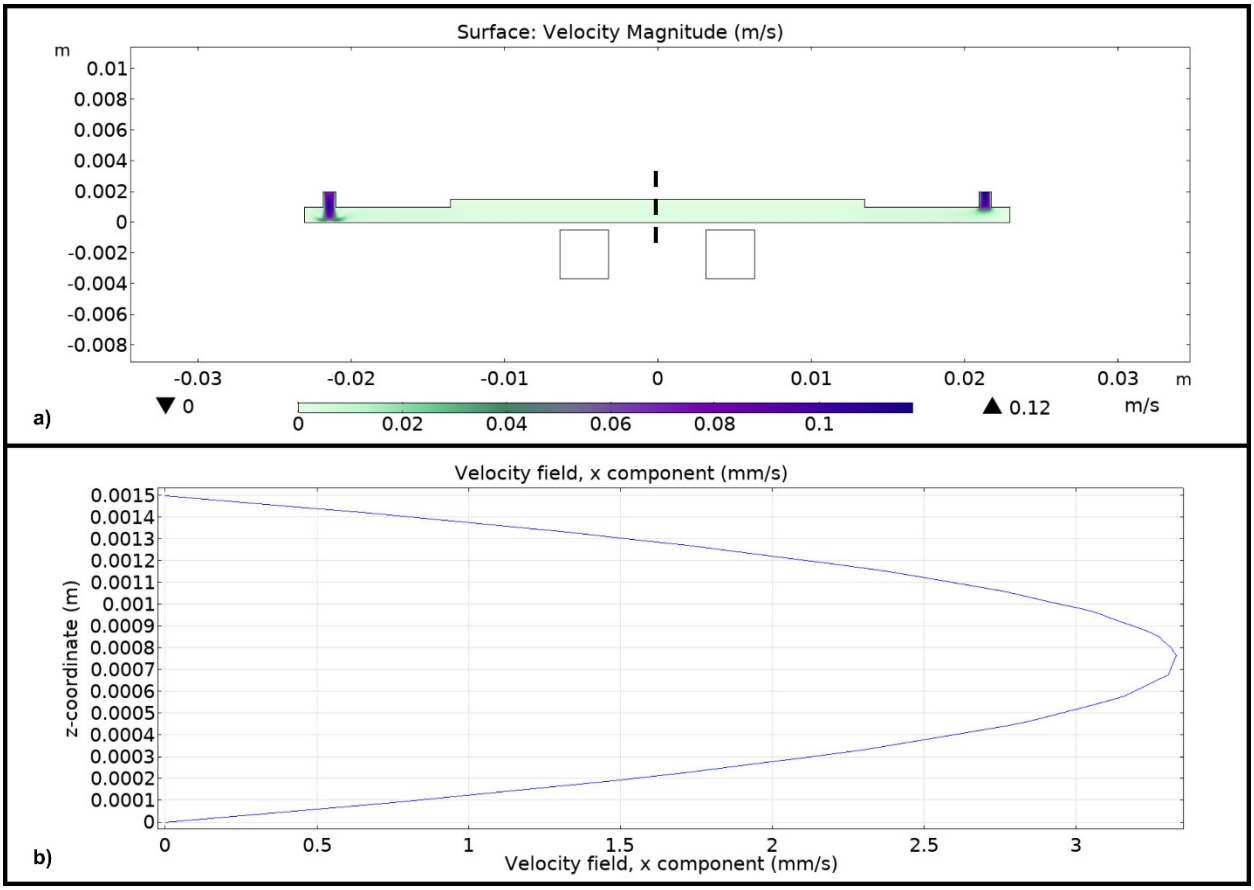

Figure 3.7. a) Flow velocity of the fluidic chamber seen from the side. b) X component of the flow velocity among the dashed line of Figure 3.7a.

The particle tracing module was used to trace the movement of the cells under the drag force and the magnetic force. Other forces such as gravity and buoyancy forces were ignored due to being at least 2 orders of magnitude lower. Coordinates of the cells when they first touch the surface of the chip due to the pull of the magnetic force were recorded. The screenshot of a typical simulation, where the cells were tracked from the instant they were introduced from the inlet of the fluidic chamber to the instant they were pulled to the surface of the chip by a ring magnet is shown in Fig 3.8a-b.

Magnets that resulted in the greatest number of cells with larger than 60 μm cell-to-cell separation were preferred since that would indicate that the cells are more likely to encounter a well (since D_{ww}=60 μm) when they reach the surface instead of encountering each other. A ring (0.5 in OD, 0.25 in ID, 0.125 in T), cylinder (0.5 in D, 0.125 in T), and a block (0.5 in L, 0.5 in, W, 0.125 in T) magnet were simulated. For each case, the distance between each cell, and the cell nearest to it are plotted. The simulation results revealed that 98%, 94%, and 87% of the cells would be more than 60 μm apart from the most adjacent cell for each magnet type respectively (Fig 3.8c-d). It was also observed by simulation that using thicker magnets would lead to more aggregation of cells as confirmed by the simulations with a ring magnet (0.5 in OD, 0.25 in ID) with varying thicknesses (0.125 in, 0.250 in, 0.375 in). The simulation results revealed that 98%, 91%, and 94% of the cells would be more than 60 μm apart from the most adjacent cell respectively (Fig 3.8e-f). Therefore, a ring magnet (K&J Magnets, R842-N52, 0.5 in OD, 0.25 in ID, 0.125 in T) was used for the experiments.

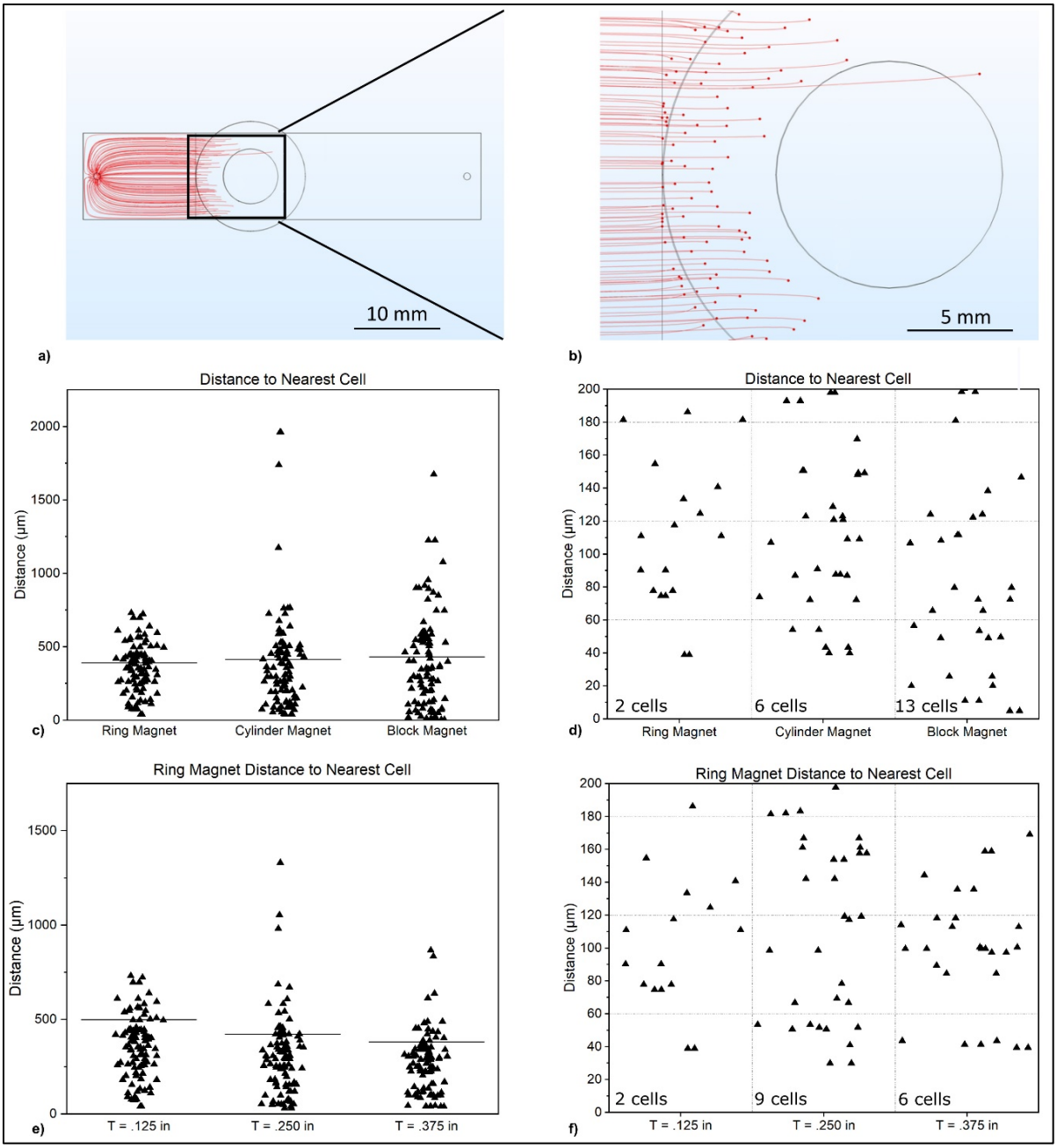

Fig 3.8. a) Distribution of the cells on the well chip with a ring magnet underneath. b) Zoomed in image of distribution of the cells on the well chip with a ring magnet underneath. c) Distance between nearest cells for ring, cylinder, and block magnets. Each data point indicates the distance between a cell and the cell nearest to it. d) Distance between nearest cells for ring, cylinder, and block magnet for distances <200 µm. e) Distance between nearest cells for ring magnets of varying thicknesses. Each data point indicates the distance between a cell and the cell nearest to it. f) Distance between nearest cells for ring magnets of varying thicknesses, for distances <200 µm. Horizontal lines on c and e indicate mean values.

4. EXPERIMENTS WITH CULTURED CELLS

4.1 Introduction

In order to characterize the operation of the system, we used JEG3 cells, a human choriocarcinoma cell line. The JEG3 has a surface antigen expression that is similar to that of circulating fetal trophoblasts and is frequently used in similar system characterization/optimization experiments [26,56].

To recognize JEG3 cells, we functionalized magnetic beads with antibodies against EpCAM (Epithelial Cell Adhesion Molecule) as well as HLA-G (Human Leukocyte Antigen G); surface antigens that are commonly used to target/verify circulating fetal trophoblasts [38,26,46,57–59]. These two antigens are commonly used due to 1) the epithelial nature of trophoblasts which warrants the targeting of EpCAM; and 2) the role of HLA-G in preventing the rejection of the trophoblasts by the maternal immune system [38,60]. The lack of these antigens on WBCs prevent the specific attachment of the functionalized beads on them. Functionalized beads were incubated with blood samples to bind to targeted cells, and the mixture was then run through the fluidic chamber that contains the porous chip with a pore dimeter of 6 μm. The well chip contained 4 groups of wells whose diameters increased from upstream to downstream: 15, 20, 30 and 60 μm. Such an arrangement ensured capturing single cells as well as clusters of cells. The wells had a uniform well depth of 20 μm which was sufficient to retain the cells in the wells and prevent them from escaping under the influence of flow. The depth of the wells was deliberately limited so as to minimize the probability of losing a cell in a well that is too deep, and to facilitate extraction by micro-pipetting. More detail on the well chip design can be found in the results section.

The immunofluorescence confirmation of the cells was accomplished by using anti-EpCAM-FITC, and anti-HLA-G-FITC antibodies. This was performed to verify that the captured cells are indeed EpCAM and/or HLA-G+. Hoechst staining was used to verify that the cells had nuclear DNA, and anti-CD-45-PE antibodies were used to identify and rule out WBCs. The choice of Hoechst allowed keeping the cells alive (vs. DAPI which requires that the cells are fixed and permeabilized). This protocol can be especially useful for applications where the cells are needed live e.g. for culturing or for assays that involve intracellular activity monitoring. For applications that do need the cells to be alive, e.g. for DNA sequencing, alternative protocols that involve fixing the cells could be used. Here, we used a micro pipette with a 50 μm tip to retrieve the cells from the well chip.

4.2 Experimental Setup

Both chambers were washed with DI water, RBS detergent (Thermo Fisher Scientific, 27950), ethanol (Thermo Fisher Scientific, A405P-4) and PBS (Thermo Fisher Scientific, 10010023) before being exposed to biological samples.

To capture cells from blood, a peristaltic pump (Ismatec, ISM596B) was used to move the sample fluid through the fluidic chamber that accommodated the porous chip. A N52 grade magnet (K&J Magnets, B444-N52) was placed to pull the target cells and the rest was collected at a waste container.

While transferring the cells from the porous chip to well chip, the outlet of our porous chip was connected directly to the inlet of the well chip, and the magnet under the porous chip was removed. A N52 grade ring magnet (with a maximum residual flux density Br_{max} of 14,800 Gauss) was

placed under the well chip (K&J Magnets, R842-N52) and the outlet of the well chip was connected to the pump (Figure 4.1a).

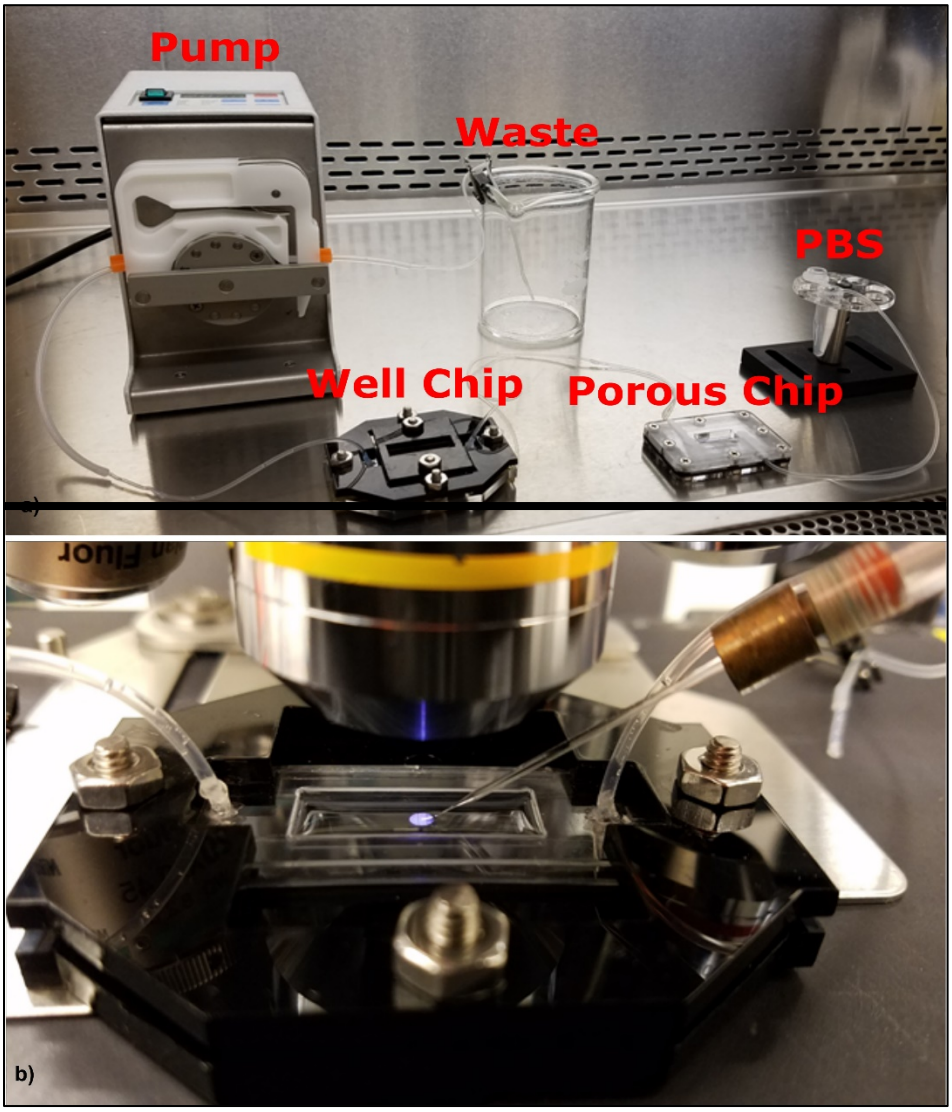

Figure 4.1 a) The bench setup while transferring cells from porous chip to well chip. b) The setup used for picking cells with the micro pipette.

A fluorescent microscope (Nikon, ECLIPSE 80i) was used to identify the target cells while a micro pipette (Clunbury Scientific, B100-58-50) was used to retrieve the desired cells (Figure 4.1b).

4.3 Culturing and the Spiking of the Cells

JEG3s were purchased from American Type Culture Collection (ATCC, HTB-36), and cultured ~~it~~ in Eagle's Minimum Essential Medium (EMEM) (ATCC, 30-2003) with 10% Fetal Bovine Serum (FBS) (ATCC, 30-2020). The cells were harvested with Trypsin-EDTA (ATCC, 30-2101), and suspended in media on a petri dish. For spiking, the cells were placed on a petri dish under a microscope and picked and spiked into blood using a micro pipette.

The blood was purchased from Biochemed Services (10761WB-EK2-FI), which had been retrieved from a single donor in a 100 ml container with EDTA anti-coagulant. The blood was stored at 4 °C until cell spiking. ~8 mL aliquots of this blood sample were used in all experiments. EDTA-containing blood collection tubes may be used if the blood sample that contains live target cells will be processed relatively quickly (hours). However, if the blood sample containing target cells need to be stored for an extended period of time (days), alternative blood collection tubes that contain preservatives (e.g. those provided by CellSave, Streck, Norgen) can be used to minimize the uncertainties that could result from possible degradation of target cells.

4.4 Detecting JEG3 Cells Spiked into Blood

For each blood sample 2 antibody-bead complexes were prepared. 17.5 µl of biotinylated anti-EpCAM antibodies (R&D Systems, BAF960) with a concentration of 0.2 mg/ml was incubated with 14 µl of streptavidin beads (Thermo Fisher Scientific, 65601) with a concentration of 10 mg/ml, and suspended in 140 µl of PBS. Also, 2 µl biotinylated anti-HLAG antibodies (Thermo Fisher Scientific, MA1-10361) with a concentration of 1 mg/mL was incubated with 8 µl of streptavidin beads (Thermo Fisher Scientific, 65601) with a concentration of 10 mg/ml, and suspended in 80 µl of PBS. Both incubations took 1 hour and were followed by a triple wash with PBS to remove any unconjugated antibodies.

The antibody-bead mixtures were incubated with 8 ml of blood for 35 mins. Afterwards the sample was diluted to 16 ml by adding 8 ml of PBS, and was run through the porous chip. The suspension was run though the porous chip 2 times, once using a flow rate of 2 ml/min and then again using 1 ml/min. The high volumetric throughput capability of the system facilitated the recirculation. This was then followed by a 4 ml PBS wash using a 1ml/min flow rate. After the wash, any remaining red blood cells were removed by a 10 min incubation with a RBC Lysis buffer (Biosciences, 786-672) followed by a 2 min PBS wash.

4.5 Immunofluorescence Analysis

Before being transferred to the well chip for analysis and retrieval, the cells were stained while they were still on the surface of the porous chip. The cells were initially stained with a mixture of anti-EpCAM-FITC (Miltenyi Biotech, 130-113-263), anti-HLAG-FITC (Miltenyi Biotech, 130-111-850), and anti-CD45-PE (Miltenyi Biotech, 130-113-118) antibodies for 15 min followed by a 4 ml PBS wash. Then, the cells were also stained with a Hoechst Solution (Thermo Fisher Scientific, 62249) for 10 mins followed by another 4 min PBS wash. This was followed by the transferring of the cells to the well chip. We identified JEG3 cells as EpCAM and/or HLAG + as well as Hoechst + (Figure 4.2 a-d).

We identified WBCs as CD45 and Hoechst + . We adopted this protocol to retrieve live cells without fixation and permeabilization, otherwise a process often used to label cytokeratin which is a protein that is inside the cell and not on its surface [57,26,46,4].

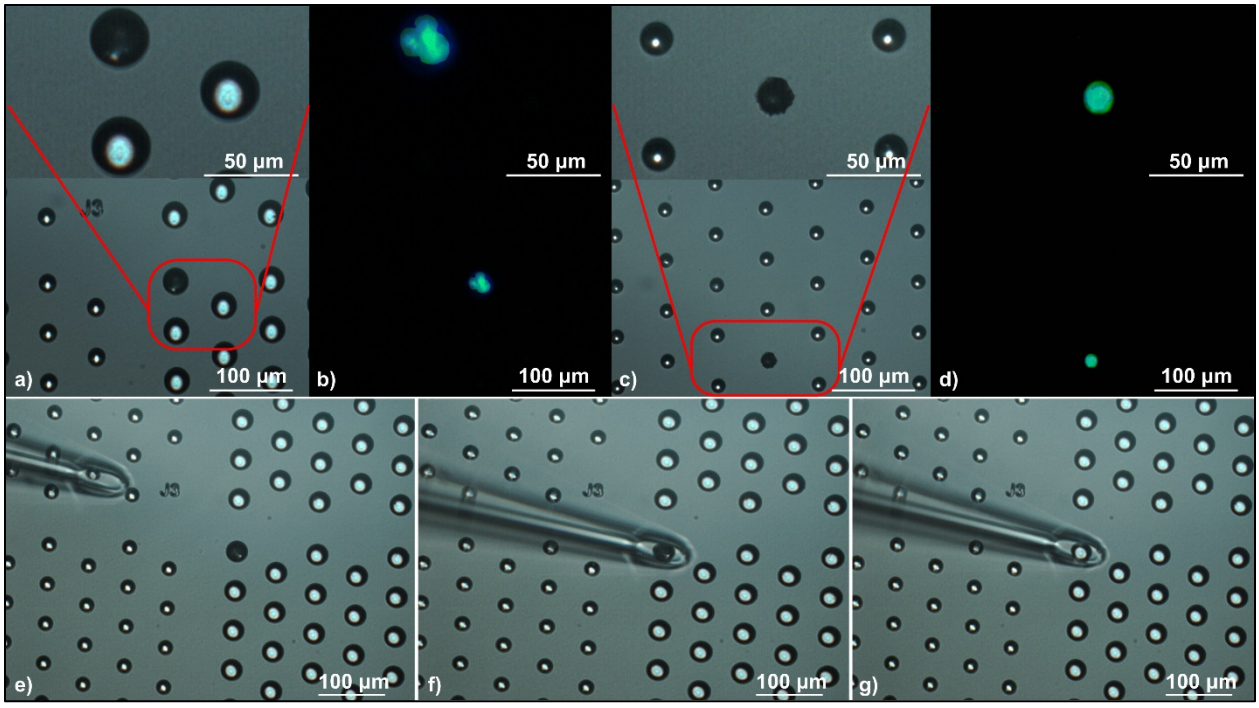

Figure 4.2 a) Bright field image of a 3 cell-cluster in a 30 µm diameter well. b) Combined anti-HLAG-FITC, anti-EPCAM-FITC, Hoechst image of the cells from Figure 4.2a. c) Bright Field image of a single cell in a 15 µm diameter well. d) Combined anti-HLAG-FITC, anti-EPCAM-FITC, Hoechst image of the cell from Figure 4.2c. e-g) Approaching and picking up of the cells from Figure 4.2 a-b with the micro pipette.

4.6 Transferring JEG3 Cells to Well Chip

In order to transfer the cells to the well chip, the magnet underneath the porous chip was removed, and the outlet of the porous chip was connected to the inlet of the well chip. The contents of the porous chip were washed into the well chip via a 2 ml PBS wash at a flow rate of 2ml/min. The cells were captured on the well chip using a ring shape magnet underneath which helped spread the cells apart from each other. When the cells first contacted the well chip surface, they all were in the vicinity of the 15 µm wells. In order to move the cells that did not initially fall into a well, as well as to move larger cell clusters into to larger wells located downstream, a magnet was brought in close proximity (approx. 2 mm) of the bottom of the well chip and slowly moved

downstream. This caused all cells to slide on the surface of the well chip until they found a well that they could fit into. Larger clusters that did not fit into the first group of wells (15 μm), continued sliding downstream until they reached 20, 30, and 60 μm wells.

4.7 Retrieval of JEG3 Cells from the Well Chip

After identifying the target cells on the well chip according to their fluorescent properties, their locations were recorded. Once the location of a cell is recorded, the fluorescence is no longer needed and the extraction can easily be performed in brightfield. Single cells were retrieved using a micro pipette with a 50 μm opening and manipulating it using a translation stage (Figure 4.2e-g).

4.8 Results and Discussion from Cultured Cells

4.8.1 Total Time of the Assay

In addition to its overall simplicity and compatibility with standard laboratory equipment, an important strength of our system is its overall speed. A single cell can be isolated from an 8 ml tube of blood and extracted in 145 mins (Table 4.1).

Table 4.1. The Timeline for the Cell Isolation and Retrieval Process.

Process	Hands On Time (min)	Total Time (min)
Incubating the target cells with Ab-Bead complex.	**1**	**35**
Detecting cells on porous chip.	**6**	**42**
Diluting blood with PBS.	2	2
Circulating the solution through the pump at 2ml/min.	1	8
Passing the solution through the pump at 1ml/min.	1	16
PBS wash.	1	4
RBC Lysis and wash.	1	12
Immunofluorescence analysis.	**4**	**33**
A-EPCAM-FITC, A-HLA-G-FITC, and A-CD45-PE staining and wash.	2	19
Hoechst staining and wash.	2	14
Transferring and locating cells on well chip.	**31**	**32**
Transfer from porous chip to well chip.	1	2
Locating cells on the well chip.	30	30
Picking up a cell from well chip.	**3**	**3**
Total	**45**	**145**

4.8.2 System Characterization

In order to characterize the performance of our system, we performed spiking experiments with 8 ml blood samples. We performed experiments using i) 10 single cells, ii) 25 single cells, and ii) 25 cells that contained known numbers of single cells as well as clusters of pairs, triplets and quadruplets. Each set of experiments was performed 3 times. We compared the number of cells

we spiked into a blood sample to that we retrieved from the well chip after the blood sample went through all of the processes described in Table 1.

In the experiments where we spiked 10 single cells into 8 ml of blood, our retrieval rates ranged from 80 to 100% with an average of 90% (see Figure 4.3a). In the experiments where we spiked 25 cells, our retrieval rates were consistently 88%. For the experiment where we spiked a combination of single cells and clusters, the successful retrieval rate varied from 84% to 96% with an average of 89.3%. (This set of experiments is denoted as "25 cells in clusters" in Figure 4.3a and shall be described with additional detail later). The overall retrieval yield between all of the aforementioned experiments was 89.1%. Lack of the CD45 stain on those cells that are positive for HLA-G/EpCAM/Hoechst, as well as the fact of consistently retrieving cells that are less than or equal to the number of spiked cells suggest that the experiments did not yield false positives.

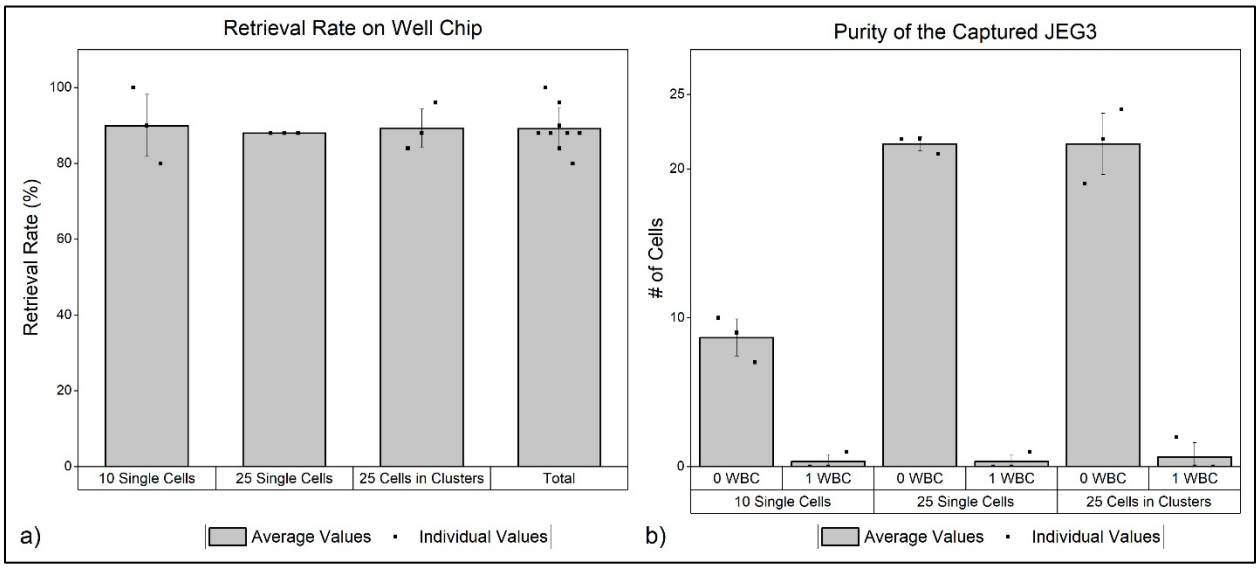

Figure 4.3. a) % Retrieval of the JEG3s. b) Purity of the captured JEG3s. # of cells refer to the target cells whereas 0 WBC and 1 WBC refer to the number of WBCs that are in the same well as the target cell.

Another way to represent the overall capture rate is by means of confidence intervals. For the nine capture rates collected from the 3 types of experiments [80, 90, 100, 88, 88, 88, 84, 88, 96] the expected mean can be calculated by using a t-distribution. This is possible because the cell capture experiments by their nature have standard distribution. The range of population mean is given with the following formula:

$$(\mu_{min}, \mu_{max}) = \bar{x} \pm t \frac{s}{\sqrt{n}}$$

Where $\bar{x}$ is the sample mean (89.1), s is the sample standard deviation (5.93) and n is the number of samples (9).

t is the t-score for a given degree of freedom (df = n-1) which is 8. Using a student t distribution table t can be found as 1.86 for a 90% confidence level. Putting all the numbers together, the population mean interval for the overall capture rate at 90% confidence interval becomes (85.42, 92.8)

We also studied the purity of the single cells we were able to retrieve (Figure 4.3b). The main contaminant in a typical rare cell detection experiment in blood is WBCs. Our system discards a great majority of the WBCs during the first (i.e. the porous chip) stage and then compartmentalizes the remaining WBCs into individual wells of the well chip to further enhance purity. Ideally, every well should be occupied by one cell only. Therefore, we investigated the extent of the imperfection in the system where a WBC accidentally co-occupies a well along with a target cell. These results are shown in Figure 4.3b for each set of experiments. We can define a 'purity percentage' as the number of target cells retrieved from a well, divided by the total number of cells in that same well. A 100% purity would indicate that a single target cell retrieved from a well had no WBCs with it.

Between the 3 experiments with 10 single cells, where we were able to retrieve a total of 27 of the 30 spiked cells, 26 of these cells had 100% purity and 1 cell had 50% purity (it co-occupied a well with a WBC and was therefore retrieved along with it). Between the 3 experiments with 25 single cells we were able to retrieve a total of 66 of the 75 spiked cells; with 65 cells with 100% purity and 1 cell with 50% purity. Finally, for the experiments with 25 cells in clusters, we were able to retrieve 67 of the spiked 75 cells; with 65 cells with 100% purity and 2 cells, each with 50% purity. For all cases with 50% purity, the well had 1 target cell and 1 WBC in it. In total, 156/160 (98%) cells retrieved had 100% purity.

In addition to assessing the total number of cells retrieved and the purity of the cells retrieved, we also investigated the ability of the system in maintaining single cells as single cells and clusters as clusters. Additionally, we kept track of the dimeter of the wells the cells were retrieved from to confirm that we could indeed move larger clusters further downstream of the well chip, while keeping the single cells confined in the smaller wells upstream.

Between the 3 experiments with 10 spiked single cells, 25 out of the 27 cells that were retrieved were in single cells form and only 2 of these single cells fell into the same well and formed a “pair” (Figure 4.4a). For the experiments with 25 spiked single cells, 62/66 cells we retrieved were in single cells form and only 2 pairs were formed on the well chip (Figure 4.4b).

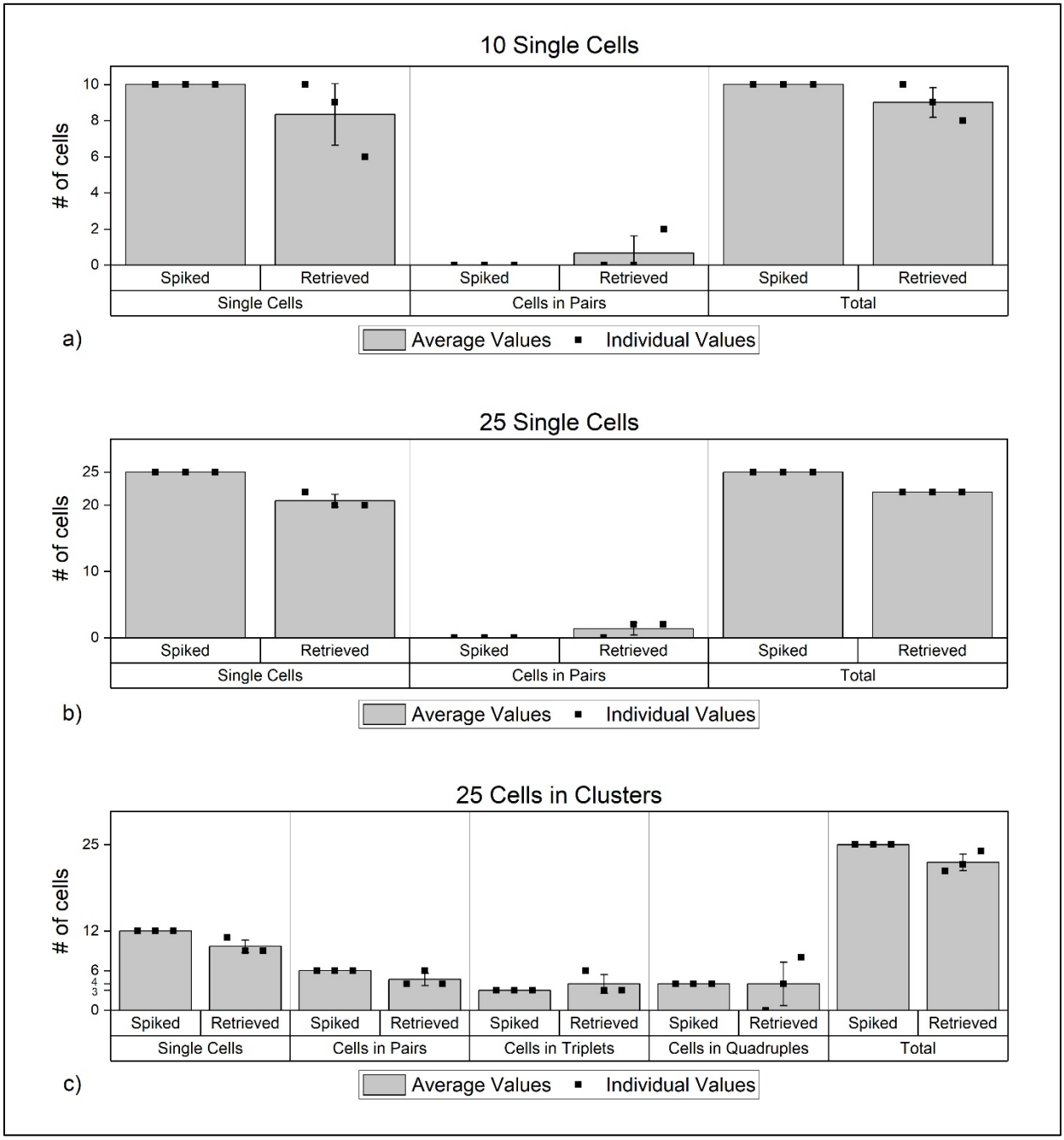

Figure 4.4. Cluster distribution data for experiments with a) 10 single cells, b) 25 single cells, c) 25 cells in clusters.

In each of the 3 experiments with “25 cells in clusters”, 12 single cells, 6 cells in pairs (i.e. 3 pairs), one triplet, and one quadruplet were spiked. Of the 12 single cells spiked, we were able to retrieve 9, 11, and 9 cells in each experiment. Of the 6 cells spiked in pairs (i.e. 3 pairs), we were able to retrieve 6, 4 and 4 cells (or 3, 2 and 2 pairs). The triplet that was spiked was retrieved as a triplet in 2 out of 3 experiments and an additional triplet was observed (i.e. 3, 6 and 3 cells in triplets were retrieved). The quadruple that was spiked was retrieved as is in one of the 3 experiments. In another experiment, no quadruple was observed in the end of the experiment. Yet in the 3rd experiment, two quadruples were observed although only one quadruple was spiked (0,4, and 8 cells in quadruplets). No clusters larger than a quadruplet was observed (Figure 4.4c).

Even though a few clusters appeared “lost”, and a few “created”, the high percentage of the total number of cells retrieved (regardless of their cluster status) suggest that those clusters may have merely disintegrated into smaller clusters during the process and then combined with smaller clusters or single cells to co-occupy a well. For example, it is highly probable that a quadruple that was carefully aspirated from the culture medium as a quadruple could have disintegrated into smaller clusters during the incubation step after it was spiked into blood sample (which is rotated for 35 mins) before it is sent into the device.

The formation of the extra clusters could also have happened at different stages of the experiments: while the cells were being incubated inside the blood tube, while they were pulled down to the porous chip, while they were being transferred from the porous chip to well chip, or while they were being dragged on the surface of the well chip by the magnet underneath. Such imperfections could be further mitigated by increasing the dimensions of the microchips and by using wider

magnets to ensure that the cells are spread out further when they are on the surfaces of the microchips.

Finally, we tracked the locations of the cells on the well chip. For the experiments with 10 single cells, the majority of the single cells were found in the 20 μm wells. Fewer cells landed in 15 μm wells (upstream of the 20 μm well) and only 1 cell in each experiment landed in a 30 μm well (Figure 4.5a). Only in one of the 3 experiments, was a pair encountered in a 20 μm well. It is possible that in this one case, a cell was fully inside the well, with its co-inhabitant partially sticking outside the well. In our experiments, we observed that as long as one of the cells fits inside a well, the pair will not move on the well chip with the movement of a magnet underneath.

For the case where 25 single cells were spiked as single cells, as well as the case where 25 cells were spiked in clusters, the results were similar to the 10 single cell experiments: more single cells in the 20 μm well, and fewer in 15 and 30 μm wells. (Figure 4.5b and c). As expected, in the experiment where 25 cells were spiked in clusters, cells in pairs and other clusters mostly settled in 30 μm wells (Figure 4.5c).

When we combine the data from 3 different experiments, we consistently observed that single cells mostly occupied 20 μm wells, while the pairs mostly occupied 20 μm and 30 μm wells. Clusters larger than pairs were all observed in wells with 30 μm diameter which demonstrates that those larger clusters were able to slide downstream on the well chip under the influence of the horizontally moving magnetic field.

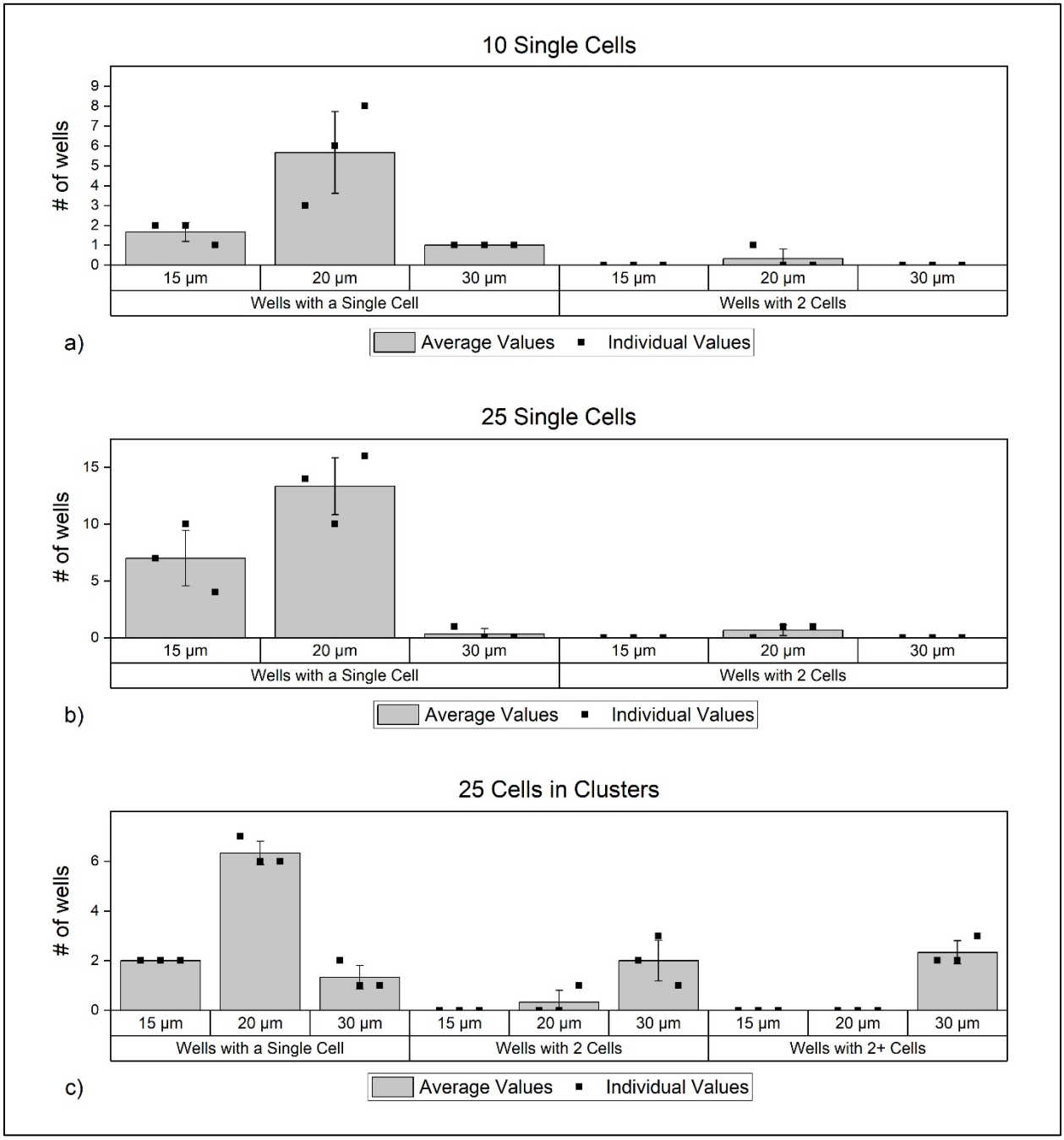

Figure 4.5. JEG3 Distribution Relative to Well Diameter for experiments with a) 10 single cells, b) 25 single cells, c) 25 cells in clusters.

5. EXPERIMENTS WITH PATIENT SAMPLES

5.1 Introduction

While the experiments with actual maternal samples were fundamentally based on those with model JEG3 cells (described earlier), some modifications were made due to the sheer fact that fetal trophoblasts are not exactly the same as JEG3s. Actual fetal trophoblasts have a weaker and less homogeneous expression of surface antigens and are more frail. In addition, the most immediate goal in capturing fetal trophoblasts is genetic sequencing which does not require the cells to remain alive after capture, which then also removes the restriction on surface-only staining. We describe this modified protocol in detail.

To capture fetal cell candidates on the surface of the porous chip, we functionalized magnetic particles with antibodies against EpCAM, and HLA-G, antigens commonly found on surfaces of circulating fetal cells. For some samples we aimed to bolster the ability to capture more cells and hence augmented the cocktail further by included Trop-2. Just like EpCAM (also called Trop-1) Trop-2 is also highly expressed in the trophoblasts of the placenta and plays an important role in embryonic and fetal development [61,62].

The immunofluorescence confirmation of the cells was accomplished by using anti-cytokeratin (CK) FITC antibody. This was done in order to maximize the fluorescent signal coming out of a target cell. While JEG3s had enough EpCAM and HLA-G expression on their surface to be both targeted by the antibody-bead complex and the fluorescent dyes; candidate fetal cells were not bright enough to be identified using proteins expressed on the surface only. CK is expressed inside many epithelial cells including trophoblasts and is responsible for providing rigidity to those cells

[63–65]. DAPI staining was used to verify that the cells had nuclear DNA, and anti-CD-45-PE antibodies were used to identify and rule out WBCs.

The experiment setup was similar to the one with JEG3 cells. Same pump, FL microscope and micropipette was used during parts of the experiment. Different steps were taken during the transfer and immunofluorescence analysis of the target cells. While transferring cells, an air bubble was utilized to transfer any cells stuck on the surface of the porous chip. Before introducing the fluorescent dye, cells were fixed and permeabilized while they were inside the wells. This step was necessary for the FL dyes to target the CK inside the cells.

5.2 Obtaining Blood Samples

Blood samples from pregnant women were obtained from Indiana University School of Medicine under an approved IRB protocol. Blood from a total of 17 patients were collected. The pregnancies were in the first trimester and the patients were approximately 6-12 weeks into their pregnancies. The volume of a sample in a tube ranged from 5-9 ml. 1 tube of blood was collected from 11 patients, and 2 tubes of blood were collected from 6 patients. Standard EDTA tubes were used in the collection and samples were processed within one day to minimize loss of cells via disintegration inside the blood collection tube.

5.3 Cell Detection on Porous Chip

To target CFCs, biotinylated EPCAM, Trop-2, and HLA-G antibodies suspended in PBS were individually incubated with streptavidin beads for an hour. This was followed by a magnetic wash with PBS which removes any unconjugated antibodies.

The antibody-bead mixtures were incubated with the tube of patient blood for 1 hour. Afterwards the sample was doubled in volume with PBS and was run through the porous chip 1 time at

1ml/min. This was followed by a 4 min PBS wash at the same flow rate. Any remaining red blood cell was were removed with a 10 min RBC Lysis buffer incubation followed by a 2 min PBS wash.

5.4 Transferring Cells from Porous Chip to Well Chip

To initiate the transfer, a well chip is connected to the outlet of the porous chip, and the outlet of the well chip was connected to the pump (where the pump 'pulls' the sample fluid into the chambers). The magnet underneath the porous chip was removed while a magnet was placed under the well chip to direct the transferred cells into wells. A 1 ml PBS wash was used to move any cells that were not stuck on the porous chip. This was followed by the introduction of an air bubble to dislodge any cells that might be stuck on the porous chip. The bubble and the dislodged content were emptied to a test tube which was then immediately introduced to the well chip (Figure 5.1). A 2 ml PBS wash was used to ensure the entirety of the volume inside the tube was transferred to the well chip. All of the transfer steps took place at 1 ml/min.

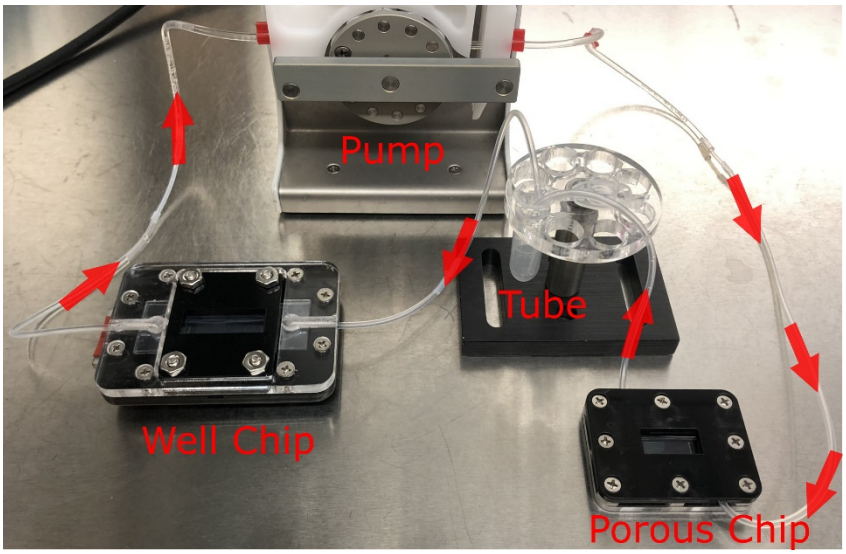

Figure 5.1. The experimental setup during the transfer of cells from porous chip to well chip. The arrows show the direction of flow.

5.5 Immunofluorescence Analysis

Once in the well chip, cells were fixed and permeabilized prior to the fluorescence staining. A 5 min incubation with a Paraformaldehyde solution 4% in PBS (Santa Cruz Biotechnology) was used to fix cells. The solution was removed with a 4 min PBS wash. Cells were permeabilized with a 10x Perm/Wash solution (BD Biosciences) for 10 mins which was similarly removed with a 4 min PBS wash. A mix of Anti-CK-FITC, anti-CD45-PE and DAPI was used to stain the cells for 10 mins flowed by a 4min PBS wash. All the wash steps took place at 1 ml/min. We identified fetal cell candidates as CK+ and DAPI+ (Figure 5.2 a-d). We identified WBCs as CD45+ and DAPI+. Anything that was DAPI- was not identified as a cell.

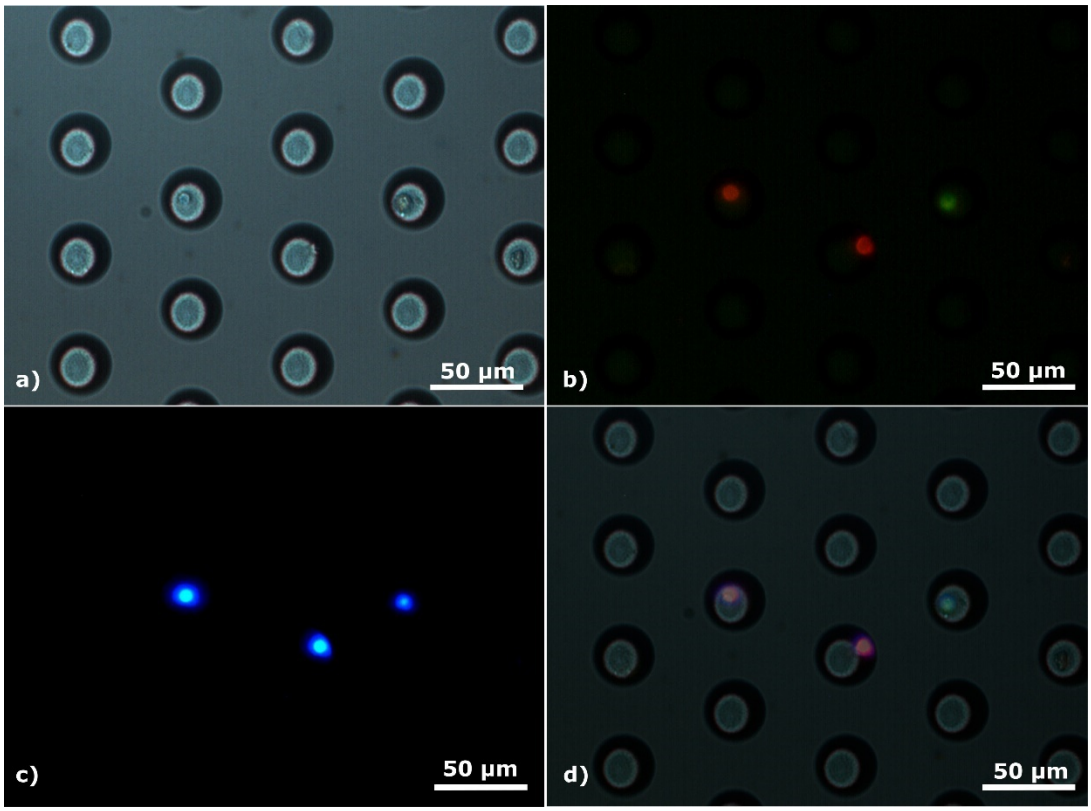

Figure 5.2. Images of one fetal cell candidate and two WBCs. a) Under bright field. b) Under fluorescent microscope with anti-CK-FITC and anti-CD45-PE dye. c) Under fluorescent microscope with DAPI dye. d) Merged image from a-c.

5.6 Cell Retrieval

After identifying the target cells on the well chip according to their fluorescent properties, their locations were recorded. Once the location of a cell is recorded, the fluorescence is no longer needed and the extraction can easily be performed in brightfield (an inherent advantage of the well chip system). Single cells were retrieved using a micro pipette with a 50 μm opening manipulated by using a translation stage.

5.7 Results and Discussion from Patient Samples

5.7.1 Total Time of the Assay

The total time needed to isolate a cell from a patient blood sample is given in Table 5.1. Compared to the 145 mins it takes to isolate a cell from the JEG3 experiments, it takes 22 more mins to isolate a single cell at a total of 167 mins.

Table 5.1. The Timeline for Experiments with Patient Samples.

Process	Hands On Time (min)	Total Time (min)
Incubating the target cells with Ab-Bead complex.	**1**	**60**
Detecting cells on porous chip.	**5**	**34**
Diluting blood with PBS.	2	2
Running the solution through the pump at 1 ml/min.	1	16
PBS wash.	1	4
RBC Lysis and wash.	1	12
Transferring Cells from Porous Chip to Well chip.	**2**	**3**
Immunofluorescence analysis.	**4**	**37**
Fixing cells.	1	9
Permeabilizing cells.	1	14
A-CK-FITC, A-CD45-PE, and DAPI staining and wash.	2	14
Locating cells on well chip.	**30**	**30**
Picking up a cell from well chip.	**3**	**3**
Total	**45**	**167**

The increased time can mostly be attributed to the 60 mins required to incubate target cells with the Ab-bead complex (compared to 35 min for JEG3 experiments). While this time can be brought down if a larger concentration of ab-beads is used to conjugate with the target cells; it would add an additional cost to the experiment. One can adjust the number of ab-beads and incubation time to optimize the cost and duration of an experiment.

The immunofluorescence analysis step takes nearly the same time (33 min for JEG3 experiments vs 37 mins for patient samples). While the addition of fixing and permeabilization steps increase the overall time of the experiment by 15 min, the ability to introduce all the fluorescent dyes in a single step and incubate for a lesser time (15 min for JEG3 vs 10 min for patient samples) causes the time difference of the immunofluorescence analysis to be only 4 mins longer for the patient samples.

The volume of a tube of blood has a high influence on the time of the experiment as well. As mentioned before a tube of blood for the experiments varied from 5-9 ml which corresponds to a diluted volume of 10-18 ml. It would take 10-18 mins to run this solution through the pump. For Table 5.1, a tube of blood is assumed to be 8 ml.

5.7.2 System Performance with Patient Samples

The distribution of number of cells collected per tube of blood is given in Figure 5.3. With this initial protocol we were able to retrieve a fetal cell candidate from 13/23 (~57%) of the tubes processed. The number of cells found in a tube ranged from 0 to 10 per tube with an average of 1.96 cells per tube and a standard deviation of 2.67.

Rare cells do not have a constant concentration in blood due to their extreme scarcity. Therefore, it's expected to obtain a wide range of target cell numbers and a relatively high standard deviation between samples. Trophoblast counts ranging from 1-33, 11-31 and standard deviations of over 7 were reported in previous studies [26,46]. Because of the high standard deviation reported by us and other studies, it is possible that inability to capture a fetal cell candidate in a patient sample is indicative of the actual lack of the said target cell in that particular blood tube. It also is possible that a few additional cells that exist in the sample are actually missed by our system/protocol.

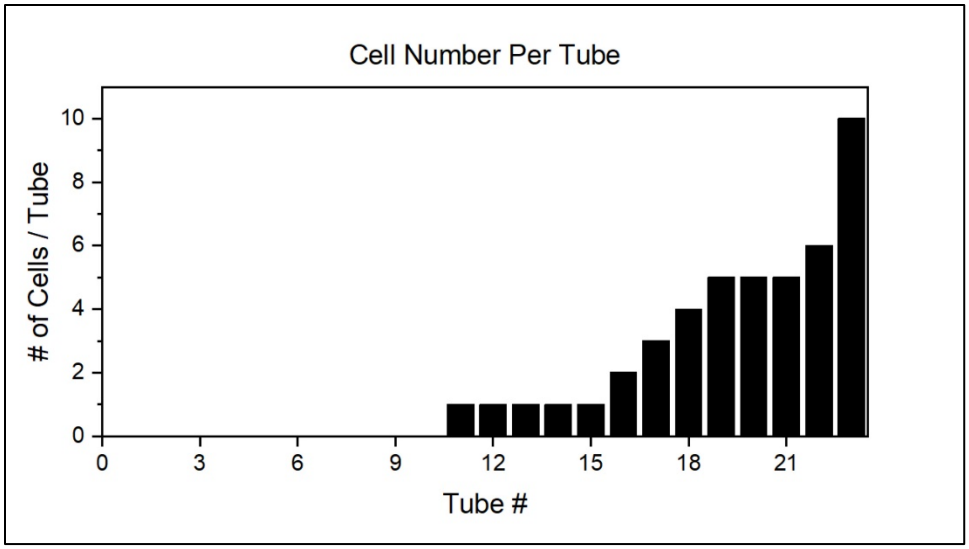

Figure 5.3. Number of fetal candidate cells obtained per tube. Each column represents a separate tube.

In Figure 5.4a, the results are separated by the number of tubes of blood processed by patient. On 11 occasions only a single tube of blood was retrieved from a patient; whereas on 6 occasions 2 tubes of blood from the same patient was processed. The average fetal cell candidates found from only 1 tube of blood was 1.7 with a standard deviation of 2; and the average fetal cell candidates found from 2 tubes was 4.33 with a standard deviation of 4.8. When these 2 categories are compared, a p value of 0.132 was found which means the averages are not significantly different at the 86.8% and higher confidence levels, even though the average of the latter was higher than the former.

The lack of a significant average difference between 1 tube and 2 tubes of processed samples are expected due to the extremely rare (on the order of 1 per billion blood cells) nature of the target cells. Further, this scarcity results in the lack of a homogeneous concentration of these cells in blood. This in turn makes it possible to sometimes obtain more cells from one tube, and fewer or

no cells even after 2 tubes are processed. Of the 11 samples processed as single tube, 4/11 (~36%) resulted in 0 cells. Of the 6 samples processed as 2 tubes, only 2/6 (~33%) cases resulted in 0 cells.

Even though the distribution of data with 1 or 2 tubes of blood were not statistically different from each other due to rather large standard deviations, the average of the latter is higher than the former, and each additional cell that is captured is extremely precious in terms of the genetic data it possesses, even if capturing more cells is not guaranteed by using 2 tubes of blood instead of 1. Our ability to quickly process large volumes of blood makes it possible for us to pursue this type of analysis with more tubes of blood and with a larger number of patients. Every additional tube of blood only adds an extra 16 minutes to the overall experiment duration which means while a tube of blood (~8 ml) takes 167 mins to process, 2 tubes would take just over 3 hours (183 mins) and so on. This gives us the flexibility to process large volumes of blood while still keeping experiment times under reasonable durations. Therefore, in the future we can expand this study to include 3 or more tubes of blood in order to retrieve a more consistent number of cells and shrink the confidence intervals.

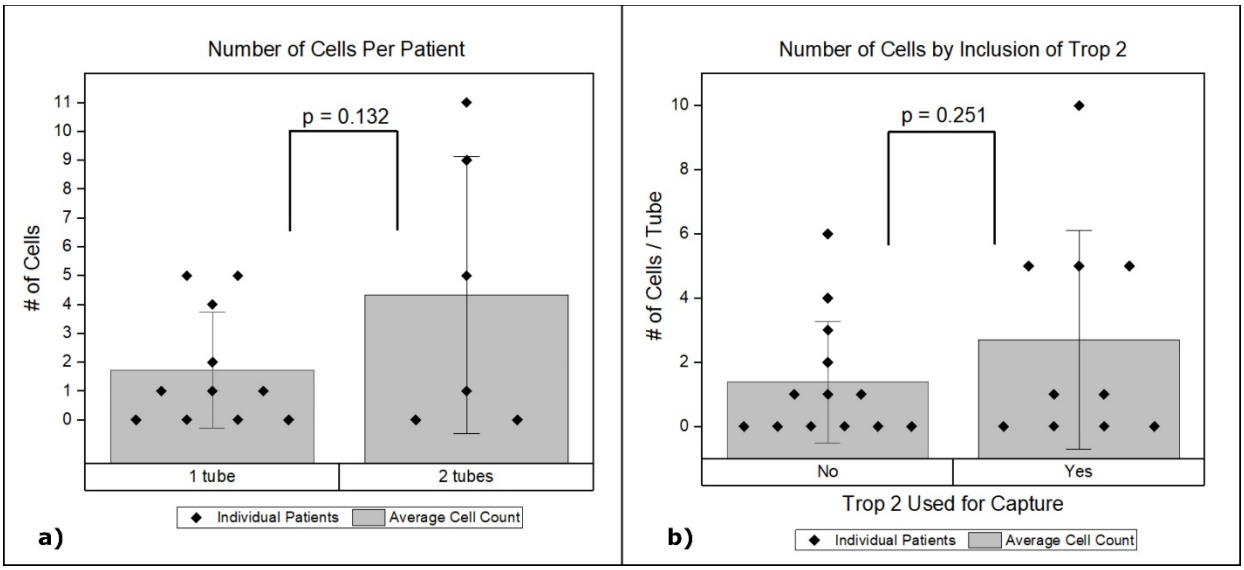

Figure 5.4. a) Number of cells per patient. Data points on column labeled "1 tube" represents number of cells obtained from patients with only a single tube of blood was processed. Data points on column "2 tube" represents the cumulative number of cells found from patients with two tubes of processed blood. b) Number of cells retrieved with respect to the presence of Trop-2 antibody in the capture antibody mixture. Each data point represents number of cells obtained from a single tube of blood. For both plots the columns represent the average values and the error bars represent standard deviation.

To demonstrate our system's ability to functionalize multiple antibodies, we added Trop-2 antibody-bead pairs to some samples in addition to the EPCAM and HLA-G antibody-bead pairs used in every other sample. The results are shown in Figure 5.4b. For samples without the use of Trop-2 an average of 1.38 cells were retrieved with a standard deviation of 1.89. For samples with Trop-2 antibodies included, an average of 2.70 cells were retrieved with a standard deviation of 3.40. When the averages of these 2 categories are compared, a p value of 0.251 was found which means the averages are not significantly different at the 74.9% and higher confidence levels.

Of the 13 samples where Trop-2 was not used, 6/13 (~46%) of the samples yielded 0 cells whereas of the 10 samples processed with the addition of Trop-2, 4/10 (~40%) of the samples yielded 0 cells.

With the advances in genetic sequencing, a single cell is all that's needed to obtain the genome of the fetus. While the differences might be low, we observed that increasing the volume of blood processed and adding additional antibodies known to be expressed by the target cells increase our chances of capturing at least one cell. While obtaining more data points would make our observations more conclusive, it's important to note that the unique engineering of our system enables us to process larger volumes and adding additional antibodies with ease, which is not applicable to all existing platforms. Therefore, further optimizations to the cell detection protocol will focus on getting at least one cell per patient by doing a combination of changing the experiment conditions to favor the capture of more cells and increasing the amount of blood obtained per patient.

The cells obtained from the patient samples are enriched by their surface protein expression of EpCAM, HLA-G, Trop-2 (when applicable) and identified as fetal cell candidates according to their expression of CK and presence of DNA content confirmed by DAPI. In order to verify the fetal origin of these candidate cells, a genomic confirmation will need to be performed that differentiates the DNA of the candidate cell from that of the mother.

6. FUTURE WORK

6.1 Sequencing of Fetal Cell Candidates

Sequencing methods come with different resolutions that affect the range of conditions that can be detected. Traditional methods such as karyotyping and fluorescence in situ hybridization have limited resolution and can detect abnormalities on the whole chromosome level to 5-10 megabase pair level [17]. While the usage of chromosomal micro array analysis (CMA) increases the resolution of detection of CNVs to kilobase levels, it still falls short of detection nucleotide level abnormalities. With next generation sequencing (NGS) however, monogenic diseases (diseases resulting from modifications in a single gene) such as Meckel-Gruber syndrome can be detected [66,67].

In addition to its ability to detect monogenic diseases, NGS is a powerful tool to differentiate fetal cell candidates from maternal cells. While our system can isolate cells based on different protein expressions on cells, non-specific binding of beads or fluorescent dyes can cause false positive identification of cells as fetal cells. In order to confirm fetal cell origin, fetal cell candidates and known maternal cells should be sequenced and compared to each other. Therefore, it's crucial for the cells we capture through our device to be compatible with NGS methods.

In order to demonstrate our system's compatibility with NGS, we used cultured JEG3 spiked into a tube of blood and isolated using our protocol for fetal cell candidate capture detailed in chapter 5. After sequencing, we used copy number variation (CNV) analysis to compare the genetic map of the JEG3 to a WBC from a healthy female.

Both the JEG3 and WBC were located on separate wells of the well chip and were identified through fluorescent dyes. The cell was released into individual PCR tubes with 5 µl of cell extraction buffer by Takara Bio.

PCR on the cell was performed with The SMARTer PicoPLEX Single Cell WGA Kit by Takara Bio following the manufacturer's instructions. The concentration of the DNA was confirmed by a nanodrop spectrometer. DNA purification was performed by DNA Clean & ConcentratorTM-25 kit by Zymo Research.

The sequencing and the bioinformatics were performed by the Purdue Center for Cancer Center. The resulting CNV scatter plot for the JEG3 is shown in Figure 6.1.

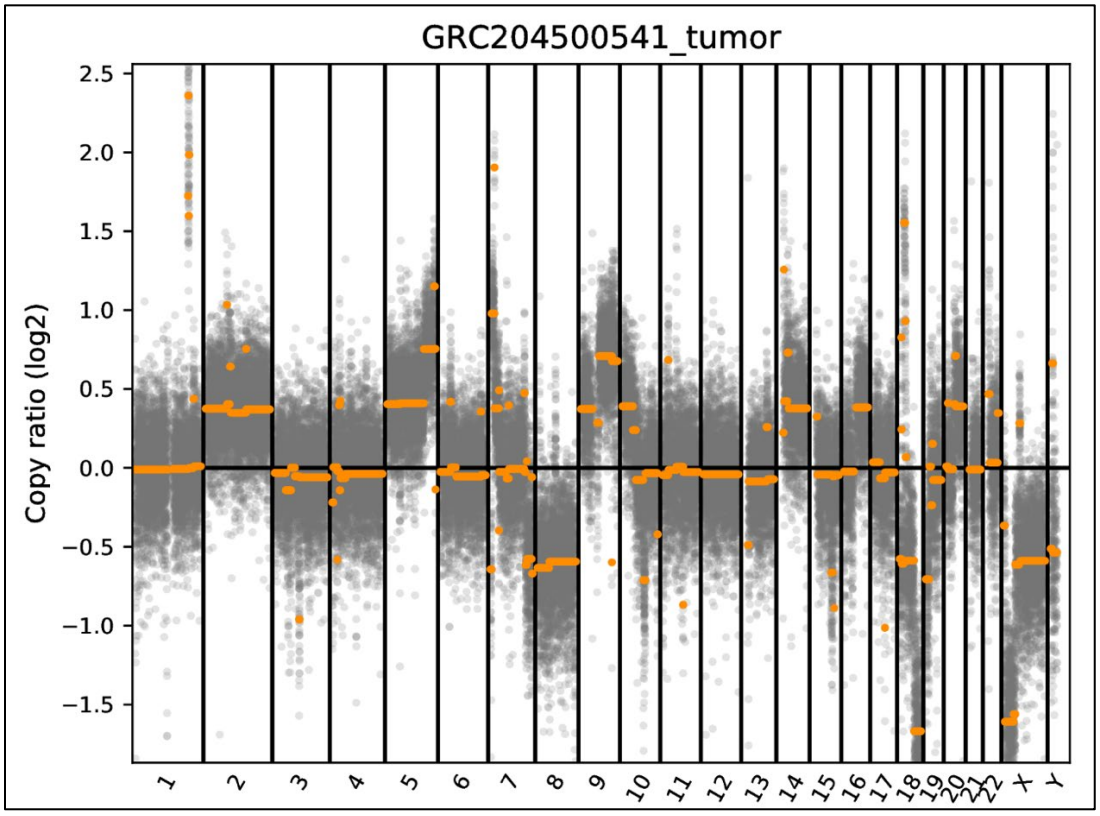

Figure 6.1. The Scatter plot of the JEG3 cell. The orange color highlights the absolute integer copy numbers on each chromosome.

The CNV plot compares the quantity of genes within chromosomes of the JEG3 to the quantities of the same genes of the WBC. A quantity of 0 in log2 scale indicates that the JEG3 cell and the WBC has the same quantity of the inspected gene. Any number below 0 suggest a deletion (loss of a gene) and any number above 0 indicates an insertion (addition of a gene) of the indicated gene.

The ability to sequence and analyze a single JEG3 cell confirms that the cells separated and collected from the well chip are indeed eligible for NGS at a single cell resolution. This makes the porous chip and well chip system compatible for any type of rare cell isolation and sequencing as long as the candidate cells have distinct biomarkers that can be targeted for detection with magnetic beads and identification with fluorescent dyes.

To confirm our device's compatibility with prenatal diagnostics, our proposed future work is to sequence the fetal cell candidates we obtained from patient samples. Once the fetal origin of the cells is confirmed, we believe our rare cell detection system can be used in clinical trials and help doctors diagnose elusive genetic conditions in fetuses.

6.2 Performance Improvements

Since the number of cells sought is extremely small, missing a single cell (from a tube that has only one) could be detrimental. Therefore, we envision that future work will be performed to enhance the performance of the system in terms of minimizing the chances of losing cells. This could involve testing various experimental conditions such as different flow rates. For example, reducing the flow rate would reduce the fluidic drag that aims to push the cells out of the chamber. The reduction in throughput caused by reducing the flow rate could then be mitigated by parallelizing the operation of the system.

An important part of the assay is the recognition of the antigens on the targeted cells. Unfortunately, in the context of fetal cells, the underlying biology of these antigens is only partially understood. Since the field of cell-based non-invasive prenatal diagnostics is new and booming, we expect significant research will be performed that will shed light on more antigens that might be present on the surfaces of fetal trophoblasts. Furthermore, higher quality antibodies, including those that are used currently (such as EpCAM, HLAG etc) can be produced while they are challenged by their ability to recognize the antigens while they are on the cells' surfaces. Currently, this is not how most antibodies are produced, instead the antibodies are selected by their ability to bind antigens in their bare molecular form (when they are not on the surface of a cell).

7. CONCLUSION

We have demonstrated the engineering and the proof of concept of a system consisting of 2 different micro chips used in sequence to enhance the purity in isolation of rare cells from blood. The first of these chips performs a bulk isolation where the majority of the unwanted cells are discarded. The second microchip, called the "well chip" then takes the cells captured by the first chip and further increases the purity by compartmentalizing them into wells where they can be retrieved in a controlled manner without interference by cells captured in other wells. The compartmentalization occurs by manipulating the cells on the well chip via a magnetic field that moves horizontally downstream and drags the cells until they encounter a well and fall in. Thanks to the robustness of the operation of the system, cells are compartmentalized simultaneously by manually moving a magnet downstream and parallel to the chip surface, eliminating the need to observe the movement of each cell sequentially. This unique design also inherently allows rapid separation of single cells from cell clusters by arranging well diameters to increase from up to downstream. We performed extensive characterization of the system to assess the overall capture yield, purity of the retrieved cells, as well as their distribution on the well chip. We were able to capture near 90% of the spiked cells, with 98% of the captured cells having 100% purity. We also demonstrated that an assay could be completed under 2.5 hours (from spiking into blood till the retrieval of a cell).

In order to demonstrate a real-world use case for our device, we present experiments done with blood samples from pregnant women. We show that we are able to retrieve candidate fetal cells under 167 minutes. We also investigate the effects of using an additional antibody to the antibody mix we use for detection, and changing the number of tubes of blood used per patient.

Future work will involve verifying the fetal origin of the cells via DNA sequencing. To that end, we have already developed a protocol for single cell sequencing and performed the initial testing on model cells. We expect this system to be highly useful in the future not only in prenatal testing but in many other indications that involve analysis of single cells.

REFERENCES

1. Chen Y, Li P, Huang P-H, Xie Y, Mai JD, Wang L, et al. Rare cell isolation and analysis in microfluidics. Lab on a Chip. 2014;14: 626. doi:10.1039/c3lc90136j

2. Dong J, Chen J, Smalley M, Zhao M, Ke Z, Zhu Y, et al. Nanostructured Substrates for Detection and Characterization of Circulating Rare Cells: From Materials Research to Clinical Applications. Adv Mater. 2020;32: 1903663. doi:10.1002/adma.201903663

3. Brinkmann F, Hirtz M, Haller A, Gorges TM, Vellekoop MJ, Riethdorf S, et al. A Versatile Microarray Platform for Capturing Rare Cells. Scientific Reports. 2015;5: 15342. doi:10.1038/srep15342

4. Masuda T, Song W, Nakanishi H, Lei W, Noor AM, Arai F. Rare cell isolation and recovery on open-channel microfluidic chip. PLOS ONE. 2017;12: e0174937. doi:10.1371/journal.pone.0174937

5. Gao Y, Yuan Z. Nanotechnology for the detection and kill of circulating tumor cells. Nanoscale research letters. 2014;9: 1–10.

6. Hajba L, Guttman A. Circulating tumor-cell detection and capture using microfluidic devices. TrAC Trends in Analytical Chemistry. 2014;59: 9–16. doi:10.1016/j.trac.2014.02.017

7. Renga B. Non invasive prenatal diagnosis of fetal aneuploidy using cell free fetal DNA. European Journal of Obstetrics & Gynecology and Reproductive Biology. 2018;225: 5–8. doi:10.1016/j.ejogrb.2018.03.033

8. Nussbaum RL, McInnes RR, Willard HF, Thompson MW, Hamosh A. Thompson & Thompson genetics in medicine. 7th ed. Philadelphia: Saunders/Elsevier; 2007.

9. Cheng W-L, Hsiao C-H, Tseng H-W, Lee T-P. Noninvasive prenatal diagnosis. Taiwanese Journal of Obstetrics and Gynecology. 2015;54: 343–349. doi:10.1016/j.tjog.2015.05.002

10. Kulkarni M, Vengalath S. Prenatal diagnosis of genetic disorders. 1995.

11. Mujezinovic FM, Alfirevic ZM. Procedure-Related Complications of Amniocentesis and Chorionic Villous Sampling: A Systematic Review. [Review]. Obstetrics & Gynecology. 2007;110: 687–694. doi:10.1097/01.AOG.0000278820.54029.e3

12. Akolekar R, Beta J, Picciarelli G, Ogilvie C, D'Antonio F. Procedure-related risk of miscarriage following amniocentesis and chorionic villus sampling: a systematic review and meta-analysis. Ultrasound in Obstetrics & Gynecology. 2015;45: 16–26. doi:10.1002/uog.14636

13. Tabor A, Vestergaard CHF, Lidegaard Ø. Fetal loss rate after chorionic villus sampling and amniocentesis: an 11-year national registry study. Ultrasound Obstet Gynecol. 2009;34: 19–24. doi:10.1002/uog.6377

14. Amorim Costa C. Non-invasive prenatal screening for chromosomal abnormalities using circulating cell-free fetal DNA in maternal plasma: Current applications, limitations and prospects. Egyptian Journal of Medical Human Genetics. 2017;18: 1–7. doi:10.1016/j.ejmhg.2016.07.004

15. Chang L, Zhu X, Li R, Wu H, Chen W, Chen J, et al. A Novel Method for Non-invasive Diagnosis of Monogenic Diseases from Circulating Fetal Cells. Prenatal Diagnosis. n/a. doi:10.1002/pd.5796

16. Kotsopoulou I, Tsoplou P, Mavrommatis K, Kroupis C. Non-invasive prenatal testing (NIPT): limitations on the way to become diagnosis. Diagnosis. 2015;2: 141–158. doi:10.1515/dx-2015-0002

17. Rezaei M, Winter M, Zander-Fox D, Whitehead C, Liebelt J, Warkiani ME, et al. A Reappraisal of Circulating Fetal Cell Noninvasive Prenatal Testing. Trends in Biotechnology. 2019;37: 632–644. doi:10.1016/j.tibtech.2018.11.001

18. Chen P-J, Teng P-C, Zhu Y, Jan YJ, Smalley M, Afshar Y, et al. Noninvasive Prenatal Diagnostics: Recent Developments Using Circulating Fetal Nucleated Cells. Curr Obstet Gynecol Rep. 2019;8: 1–8. doi:10.1007/s13669-019-0254-x

19. Wachtel SS, Shulman Lp, Sammons D. Fetal cells in maternal blood. Clinical Genetics. 2001;59: 74–79. doi:10.1034/j.1399-0004.2001.590202.x

20. Chen Fang, Liu Ping, Gu Ying, Zhu Zhu, Nanisetti Amulya, Lan Zhangzhang, et al. Isolation and whole genome sequencing of fetal cells from maternal blood towards the ultimate non-invasive prenatal testing. Prenatal Diagnosis. 2017;37: 1311–1321. doi:10.1002/pd.5186

21. Bianchi DW, Williams JM, Sullivan LM, Hanson FW, Klinger KW, Shuber AP. PCR quantitation of fetal cells in maternal blood in normal and aneuploid pregnancies. Am J Hum Genet. 1997;61: 822–829.

22. Krabchi K, Gros-Louis F, Yan J, Bronsard M, Massé J, Forest J-C, et al. Quantification of all fetal nucleated cells in maternal blood between the 18th and 22nd weeks of pregnancy using molecular cytogenetic techniques. Clinical Genetics. 2001;60: 145–150. doi:10.1034/j.1399-0004.2001.600209.x

23. Chang C, Jalal S, Huang W, Mahmood A, Matei D, Savran C. High-throughput Immunomagnetic Cell Detection using a Micro-aperture Chip System. 2014 [cited 11 Sep 2014]. Available: http://ieeexplore.ieee.org/xpls/abs_all.jsp?arnumber=6808412

24. Chang C-L, Huang W, Jalal SI, Chan B-D, Mahmood A, Shahda S, et al. Circulating tumor cell detection using a parallel flow micro-aperture chip system. Lab Chip. 2015 [cited 27 Feb 2015]. doi:10.1039/C5LC00100E

25. Kavanagh DM, Kersaudy-Kerhoas M, Dhariwal RS, Desmulliez MPY. Current and emerging techniques of fetal cell separation from maternal blood. Journal of Chromatography B. 2010;878: 1905–1911. doi:10.1016/j.jchromb.2010.05.007

26. Hou S, Chen J-F, Song M, Zhu Y, Jan YJ, Chen SH, et al. Imprinted NanoVelcro Microchips for Isolation and Characterization of Circulating Fetal Trophoblasts: Toward Noninvasive Prenatal Diagnostics. ACS Nano. 2017;11: 8167–8177. doi:10.1021/acsnano.7b03073

27. Breman AM, Chow JC, U'Ren L, Normand EA, Qdaisat S, Zhao L, et al. Evidence for feasibility of fetal trophoblastic cell-based noninvasive prenatal testing. Prenatal Diagnosis. 2016;36: 1009–1019. doi:10.1002/pd.4924

28. Grati FR, Malvestiti F, Ferreira JCPB, Bajaj K, Gaetani E, Agrati C, et al. Fetoplacental mosaicism: potential implications for false-positive and false-negative noninvasive prenatal screening results. Genetics in Medicine. 2014;16: 620–624. doi:10.1038/gim.2014.3

29. Antfolk M, Laurell T. Continuous flow microfluidic separation and processing of rare cells and bioparticles found in blood – A review. Analytica Chimica Acta. 2017;965: 9–35. doi:10.1016/j.aca.2017.02.017

30. Hu X, Bessette PH, Qian J, Meinhart CD, Daugherty PS, Soh HT. Marker-specific sorting of rare cells using dielectrophoresis. Proc Natl Acad Sci U S A. 2005;102: 15757–15761. doi:10.1073/pnas.0507719102

31. Gee AP, Durett AG. Cell sorting for therapeutic applications -- points to consider. Cytotherapy. 2009 [cited 12 Oct 2020]. Available: https://www.tandfonline.com/doi/pdf/10.1080/14653240231725160 8?needAccess=true

32. Bianchi DW, Flint AF, Pizzimenti MF, Knoll JH, Latt SA. Isolation of fetal DNA from nucleated erythrocytes in maternal blood. Proc Natl Acad Sci U S A. 1990;87: 3279–3283.

33. Jamshaid T, Neto ETT, Eissa MM, Zine N, Kunita MH, El-Salhi AE, et al. Magnetic particles: From preparation to lab-on-a-chip, biosensors, microsystems and microfluidics applications. TrAC Trends in Analytical Chemistry. 2016;79: 344–362. doi:10.1016/j.trac.2015.10.022

34. Gerges N, Rak J, Jabado N. New technologies for the detection of circulating tumour cells. Br Med Bull. 2010;94: 49–64. doi:10.1093/bmb/ldq011

35. Sitar G, Manenti L, Farina A, Lanati V, Mascheretti P, Forabosco A, et al. Characterization of the biophysical properties of human erythroblasts as a preliminary step to the isolation of fetal erythroblasts from maternal peripheral blood for non invasive prenatal genetic investigation. 1. 1997;82: 5–10. doi:10.3324/%x

36. Calabrese G, Baldi M, Fantasia D, Teresa Sessa M, Kalantar M, Holzhauer C, et al. Detection of chromosomal aneuploidies in fetal cells isolated from maternal blood using single-chromosome dual-probe FISH analysis. Clinical Genetics. 2011;82: 131–139. doi:10.1111/j.1399-0004.2011.01775.x

37. Calabrese Giuseppe, Fantasia Donatella, Alfonsi Melissa, Morizio Elisena, Celentano Claudio, Guanciali Franchi Paolo, et al. Aneuploidy screening using circulating fetal cells in maternal blood by dual-probe FISH protocol: a prospective feasibility study on a series of 172 pregnant women. Molecular Genetics & Genomic Medicine. 2016;4: 634–640. doi:10.1002/mgg3.249

38. Vona G, Béroud C, Benachi A, Quenette A, Bonnefont JP, Romana S, et al. Enrichment, Immunomorphological, and Genetic Characterization of Fetal Cells Circulating in Maternal Blood. The American Journal of Pathology. 2002;160: 51–58. doi:10.1016/S0002-9440(10)64348-9

39. Mohamed H, Turner JN, Caggana M. Biochip for separating fetal cells from maternal circulation. Journal of Chromatography A. 2007;1162: 187–192. doi:10.1016/j.chroma.2007.06.025

40. Mohamed H, Turner JN, Caggana M. Biochip for separating fetal cells from maternal circulation. Journal of Chromatography A. 2007;1162: 187–192. doi:10.1016/j.chroma.2007.06.025

41. Byeon Y, Ki C-S, Han K-H. Isolation of nucleated red blood cells in maternal blood for Non-invasive prenatal diagnosis. Biomed Microdevices. 2015;17: 118. doi:10.1007/s10544-015-0021-3

42. Winter M, Hardy T, Rezaei M, Nguyen V, Zander-Fox D, Warkiani ME, et al. Isolation of Circulating Fetal Trophoblasts Using Inertial Microfluidics for Noninvasive Prenatal Testing. Advanced Materials Technologies. 2018;3: 1800066. doi:10.1002/admt.201800066

43. Kølvraa S, Singh R, Normand EA, Qdaisat S, Veyver IB van den, Jackson L, et al. Genome-wide copy number analysis on DNA from fetal cells isolated from the blood of pregnant women. Prenatal Diagnosis. 2016;36: 1127–1134. doi:10.1002/pd.4948

44. Liu MC, Sun Y, Ramirez A, Campton D, George T, Haselkorn KE, et al. A novel six-parameter assay for comprehensive phenotyping of circulating tumor cells. : 1.

45. He Z, Guo F, Feng C, Cai B, Lata JP, He R, et al. Fetal nucleated red blood cell analysis for non-invasive prenatal diagnostics using a nanostructure microchip. Journal of Materials Chemistry B. 2017;5: 226–235. doi:10.1039/C6TB02558G

46. Huang C-E, Ma G-C, Jou H-J, Lin W-H, Lee D-J, Lin Y-S, et al. Noninvasive prenatal diagnosis of fetal aneuploidy by circulating fetal nucleated red blood cells and extravillous trophoblasts using silicon-based nanostructured microfluidics. Mol Cytogenet. 2017;10. doi:10.1186/s13039-017-0343-3

47. Ma G-C, Lin W-H, Huang C-E, Chang T-Y, Liu J-Y, Yang Y-J, et al. A Silicon-based Coral-like Nanostructured Microfluidics to Isolate Rare Cells in Human Circulation: Validation by SK-BR-3 Cancer Cell Line and Its Utility in Circulating Fetal Nucleated Red Blood Cells. Micromachines (Basel). 2019;10. doi:10.3390/mi10020132

48. Chun-Li Chang, Jalal SI, Wanfeng Huang, Mahmood A, Matei DE, Savran CA. High-Throughput Immunomagnetic Cell Detection Using a Microaperture Chip System. IEEE Sensors J. 2014;14: 3008–3013. doi:10.1109/JSEN.2014.2321167

49. Huang W. Concurrent detection and isolation of cellular and molecular biomarkers. Purdue University. 2016.

50. Prinyakupt J, Pluempitiwiriyawej C. Segmentation of white blood cells and comparison of cell morphology by linear and naïve Bayes classifiers. Biomed Eng Online. 2015;14. doi:10.1186/s12938-015-0037-1

51. Sun T. Atlas of Hematologic Neoplasms. Springer US; 2009. doi:10.1007/978-0-387-89848-3

52. Pankhurst QA, Connolly J, Jones SK, Dobson J. Applications of magnetic nanoparticles in biomedicine. J Phys D: Appl Phys. 2003;36: R167–R181. doi:10.1088/0022-3727/36/13/201

53. Fonnum G, Johansson C, Molteberg A, Mørup S, Aksnes E. Characterisation of Dynabeads® by magnetization measurements and Mössbauer spectroscopy. Journal of Magnetism and Magnetic Materials. 2005;293: 41–47. doi:10.1016/j.jmmm.2005.01.041

54. Grob DT, Wise N, Oduwole O, Sheard S. Magnetic susceptibility characterisation of superparamagnetic microspheres. Journal of Magnetism and Magnetic Materials. 2018;452: 134–140. doi:10.1016/j.jmmm.2017.12.007

55. Gijs MAM. Magnetic bead handling on-chip: new opportunities for analytical applications. Microfluidics and Nanofluidics. 2004 [cited 17 Feb 2019]. doi:10.1007/s10404-004-0010-y

56. Wadsack C, Hrzenjak A, Hammer A, Hirschmugl B, Levak-Frank S, Desoye G, et al. Trophoblast-like human choriocarcinoma cells serve as a suitable in vitro model for selective cholesteryl ester uptake from high density lipoproteins. European Journal of Biochemistry. 2003;270: 451–462. doi:10.1046/j.1432-1033.2003.03394.x

57. Hatt L, Brinch M, Singh R, Møller K, Lauridsen RH, Uldbjerg N, et al. Characterization of Fetal Cells from the Maternal Circulation by Microarray Gene Expression Analysis - Could the Extravillous Trophoblasts Be a Target for Future Cell-Based Non-Invasive Prenatal Diagnosis? Fetal Diagnosis and Therapy. 2014;35: 218–227. doi:10.1159/000356073

58. Simpson JL, Elias S. Isolating fetal cells in maternal circulation for prenatal diagnosis. Prenatal Diagnosis. 14: 1229–1242. doi:10.1002/pd.1970141308

59. Singh R, Hatt L, Ravn K, Vogel I, Petersen OB, Uldbjerg N, et al. Fetal cells in maternal blood for prenatal diagnosis: a love story rekindled. Biomarkers in Medicine. 2017;11: 705–710. doi:10.2217/bmm-2017-0055

60. Kovats S, Main EK, Librach C, Stubblebine M, Fisher SJ, DeMars R. A Class I Antigen, HLA-G, Expressed in Human Trophoblasts. Science. 1990;248: 220–223.

61. Lipinski M, Parks DR, Rouse RV, Herzenberg LA. Human trophoblast cell-surface antigens defined by monoclonal antibodies. Proc Natl Acad Sci U S A. 1981;78: 5147–5150.

62. McDougall ARA, Tolcos M, Hooper SB, Cole TJ, Wallace MJ. Trop2: From development to disease. Developmental Dynamics. 2015;244: 99–109. doi:10.1002/dvdy.24242

63. Daya D, Sabet L. The Use of Cytokeratin as a Sensitive and Reliable Marker for Trophoblastic Tissue. Am J Clin Pathol. 1991;95: 137–141. doi:10.1093/ajcp/95.2.137

64. Maldonado-Estrada J, Menu E, Roques P, Barré-Sinoussi F, Chaouat G. Evaluation of Cytokeratin 7 as an accurate intracellular marker with which to assess the purity of human placental villous trophoblast cells by flow cytometry. J Immunol Methods. 2004;286: 21–34. doi:10.1016/j.jim.2003.03.001

65. Mühlhauser J, Crescimanno C, Kasper M, Zaccheo D, Castellucci M. Differentiation of human trophoblast populations involves alterations in cytokeratin patterns. J Histochem Cytochem. 1995;43: 579–589. doi:10.1177/43.6.7539466

66. Jones D, Fiozzo F, Waters B, McKnight D, Brown S. First-trimester diagnosis of Meckel–Gruber syndrome by fetal ultrasound with molecular identification of CC2D2A mutations by next-generation sequencing. Ultrasound in Obstetrics & Gynecology. 2014;44: 719–721. doi:10.1002/uog.13381

67. Vissers LELM, Gilissen C, Veltman JA. Genetic studies in intellectual disability and related disorders. Nat Rev Genet. 2016;17: 9–18. doi:10.1038/nrg3999

APPENDIX. MATLAB CODE FOR DISTANCE CALCULATION

```
% calculates the distance between each cell and the cell closest to it
%from a file that has the x coordinates of a cell followed by the
%y coordinates

clear all

[fileid,path] = uigetfile('*.txt');
file = fopen(fileid);

content = textscan(file, '%f');
fclose(file);
data = cell2mat(content);
N = numel(data);
N1 = ((N-1)/2);
dx = zeros(1,N1);
dy = zeros(1,N1);

dx=data(2:(N1+1));
dy=data(N1+2:N);
dxrange = sort(dx);

dist=zeros(N1,N1);
for n = 1:N1
   for m = 1:N1
      d1 = dx(n) - dx(m);
      d2 = dy(n) - dy(m);
      dist(n,m) = sqrt(d1^2+d2^2);
   end
    %n = n+1;
end

dist(dist==0) = NaN;
min_dist = min(dist);
min_dist = sort(min_dist);
average = mean(min_dist);

file = fopen(fileid,'at');
fprintf(file, '\nResults\n\n');
fprintf(file, '%f\n', min_dist);
fprintf(file, '\nAverage distance is: %f\n', average);
fclose(file);
```

VITA

Onur Gur received his B.S. degree in Electrical Engineering from University of Illinois Urbana Champaign in 2014. He is currently working toward his Ph.D. degree in the School of Electrical Engineering at Purdue University, where his research involves biosensors, bioMEMS and bioinstrumentation.